ACS NANO

www.acsnano.org

REVIEW

Ultrafast Thermal Engineering in Energy Materials: Design, Recycling, and Future Directions

Pandeng Zhao, Xingqiao Wu,* Yinghao Zhang, Wenjie Huang, Yuhai Dou, Hua Kun Liu,* Shixue Dou, Minghong Wu,* and Shulei Chou*

Cite This: https://doi.org/10.1021/acsnano.5c04768

Read Online

ACCESS | Metrics & More | Article Recommendations

ABSTRACT: Energy materials are essential for addressing global energy challenges, and their design, recycling, and performance optimization are critical for sustainable development. To efficiently rise to this occasion, advanced technology should be explored to address these challenges. This review focuses on the potential of ultrafast thermal engineering as an innovative approach to the design and recycling of energy materials and systematically examines ultrahigh temperature shock's origins, mechanisms, and developmental progress, clarifying fundamental differences between the Joule heating and carbothermal shock modes. Recent advancements in lithium/sodium battery electrode fabrication, catalyst synthesis, and battery recycling by this technology are comprehensively summarized to highlight the processing parameters, structural modulation mechanisms, and underlying principles. The review also explores the mechanisms of ultrahigh temperature shock processes, their scalability, and their environmental and economic implications. Notably, a mechanistic insight into the dynamic coexistence of Joule heating and carbothermal shock in UTS is proposed, which may synergistically govern structural evolution in poor conductivity/insulating materials. This review ultimately aims to drive the development and application of ultrafast thermal engineering in the energy materials field.

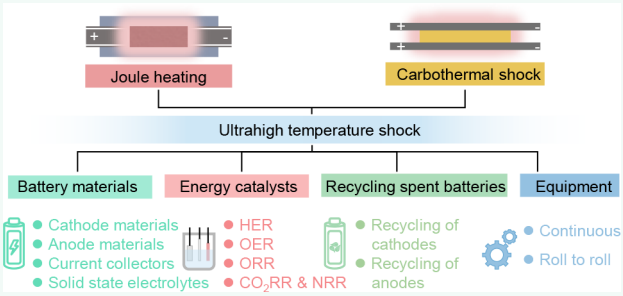

KEYWORDS: *Ultrahigh temperature shock, Joule heating, Carbothermal shock, Nonequilibrium thermodynamics, Energy materials, Batteries, Catalysis, Recycling, Scale-up equipment, Environmental and economic analysis*

1. INTRODUCTION

In recent decades, emerging energy conversion systems have vastly actuated the development of renewable energy sources and society. The growing demands for portable equipment, electric vehicles, energy storage stations, water splitting, and so on have drawn intense attention for more efficient and cheap energy conversion and storage devices. Nevertheless, most effective energy devices rely heavily on state-of-the-art energy materials, implying that developing more advanced energy materials with enhanced properties and recycling of the vast amount of retired energy materials will give rise to a formidable challenge in the future. In response, economically viable technology that allows the preparation and recycling of energy materials is necessary.

Extensive efforts have been devoted to developing novel energy materials with regulated morphologies, compositions, and sizes through conventional strategies such as solvothermal, furnace-assisted calcination, and recycling of scrapped energy materials through similar methods. However, these conventional methods often encountered ample hurdles such as thermodynamic restriction, particle agglomeration, metastable materials, and complicated synthesis steps. Importantly, with respect to energy consumption, requiring time, labor-intensiveness, and research efficiency, conventional methods are still inefficient for effective demands. To conquer these obstacles, the effective ultrahigh temperature shock (UTS) methods[1,2] based on ultrafast thermal engineering that can provide extraordinary kinetic processes and break the equilibrium limitation through transient heating and quenching

Received: March 19, 2025
Revised: April 22, 2025
Accepted: April 23, 2025

patterns have garnered intriguing attention for applying to the preparation and recycling of energy materials (Figure 1). In

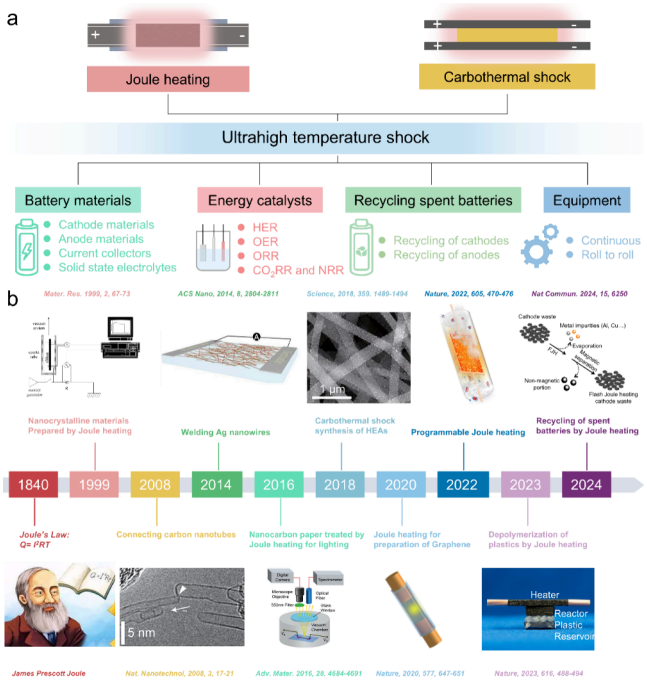

Figure 1. Overview of ultrahigh temperature shock. (a) Two main types of ultrahigh temperature shock and their applications. (b) The development and application routes of ultrahigh temperature shock. (b) Reproduced with permission.[4] Copyright 1999, SciELO Brazil. Reproduced with permission.[5] Copyright 2014, American Chemical Society. Reproduced with permission.[1] Copyright 2018, American Association for the Advancement of Science. Reproduced with permission.[3] Copyright 2022, Springer Nature. Reproduced with permission.[6] Copyright 2024, Springer Nature. Reproduced with permission.[7] Copyright 2008, Springer Nature. Reproduced with permission.[8] Copyright 2016, Wiley. Reproduced with permission.[2] Copyright 2020, Springer Nature. Reproduced with permission.[9] Copyright 2023, Springer Nature.

comparison with traditional furnace (TF) methods, the UTS method can easily synthesize or recycle materials within extremely short timeframes (milliseconds or seconds) under ultrahigh temperatures, and the solvent is not involved in this process, thus not only reducing the labor intensity and improving the efficiency of research and development but also lessening the environmental pollution from the solvent.[3] Additionally, the kinetically unfavorable reactions that cannot be carried out at conventional conditions (e.g. furnace heating and cooling at atmospheric pressure) may become a possibility through the UTS technique, such as generating a metastable state or inundant structural defects, inducing unexpected performance. Therefore, the UTS technology is regarded as an anticipant strategy for considering the time-cost, energy consumption, and efficiency of developing novel energy materials and recycling obsolete energy materials.

As a burgeoning technology and research direction for energy materials, a comprehensive understanding of the recent development of UTS technology is critical to improving efficiency and reducing the cost of preparation and recycling of energy materials. However, an overall review of the UTS technique and its application in energy materials is still lacking. Especially, the difference between Joule heating and carbothermal shock is not clear enough to be confused. Thus, it is imperative to urgently summarize recent research concerning this technology for driving the application of innovative methods. Herein, the origin, underlying mechanism, and development of UTS and the difference between Joule heating and carbothermal shock are introduced in detail. Subsequently, the specific methods, pivotal factors affecting materials structure, and current mechanism of UTS methods during the preparation and recycling of energy materials are emphatically discussed from the preparation of lithium/sodium battery electrode materials and catalysts and recycling of battery electrode materials. Besides, the scale-up equipment and environmental and economic benefits of the UTS technique are further described, providing some novel strategies for more extensive application in a wider field. Lastly, the perspective, current challenges, and double effect of dynamic Joule heating and carbothermal shock in UTS technology are proposed, which will provide future research directions and accelerate the development of the UTS technique in materials. Overall, this review aims to offer a comprehensive understanding of the UTS technique for researchers and broaden their insights to develop the UTS into scale-up and practical applications in the future.

2. ULTRAFAST THERMAL ENGINEERING

2.1. Development of Ultrahigh-Temperature Shock.

Despite Joule's law ($Q = I^2Rt$, where Q, I, R, and t represent the heat quantity, electric current, conductor's resistance, and time taken, respectively) having been proposed for more than a century, Joule heating or Ohmic heating is generally applied in traditional external furnaces in which heat is distributed throughout the furnaces, resulting in a limitation of heat transfer and low electric utilization. Thus, a strategy of direct Joule heating of the target is proposed,[8] which provides an instantaneous heating rate ($\sim 10^5$ K s^{-1}) to ultrahigh temperature ($\sim$3000 K) on reaction precursors within transient time while it is accompanied by a super cooling rate ($\sim 10^4$ K s^{-1}). The extremely remarkable conditions of UTS allow it to achieve reactions that are nearly inaccessible to traditional furnaces (Figure 2). A fast-heating rate can decompose the metal precursor to construct a highly supersaturated state, thus minimizing the nucleation barrier to generate small nuclei. Subsequently, a quick cooling can be conducted to quench small nuclei from further growth, leading to smaller particles (Figure 3a). The rapid cooling rate providing an extremely low-temperature condition also offers favorable reaction kinetics to induce the formation of fine-grained and more defects and metastable nanostructures (Figure 3b). Besides, the wide miscibility gaps in the many metallic systems impede the homogeneous structure form. Traditional furnaces cannot provide sufficient thermodynamics to synthesize favorable structures. UTS can overcome the immiscibility of metallic materials to construct a homogeneous alloy (Figure 3c). For the fabrication of high-entropy alloys (HEAs) (Figure 3d), the ultrahigh temperature in the reaction zone can compel the metal precursors to undergo drastic decomposition, resulting in vast nucleation and abundant defects, while the short (seconds, even milliseconds) reaction time at high temperature suppresses the further growth of grain and element transfer to prevent the aggeneration of nano-clusters or nanoparticles. Notably, the highly controllable temperature, time, and reaction target zone are crucial for the thermal treatment of temperature-sensitive materials. The

https://doi.org/10.1021/acsnano.5c04768
ACS Nano XXXX, XXX, XXX−XXX

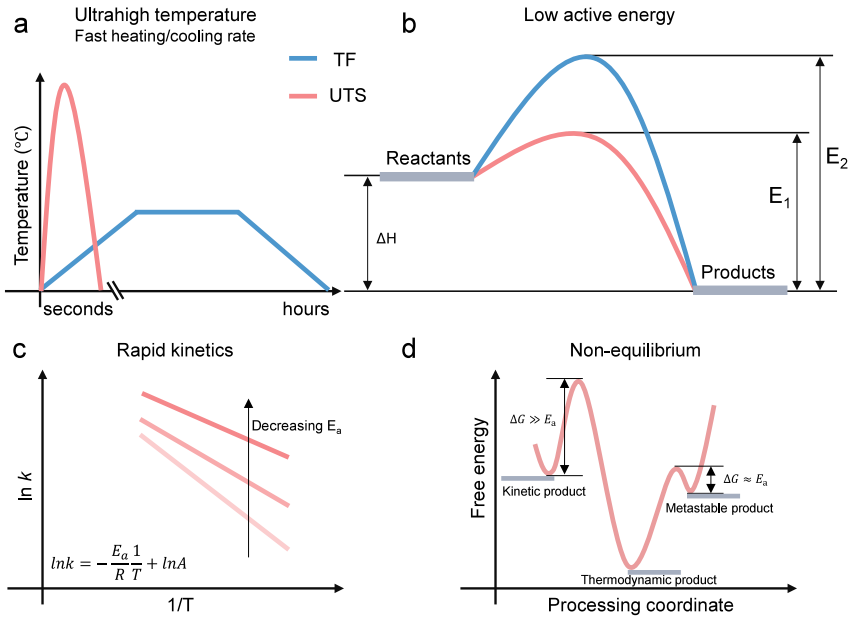

Figure 2. Characteristics and advancements of UTS compared to the TF method: (a) fast heating/cooling rate and ultrahigh temperature, (b) lower active energy, (c) faster reaction kinetics, and (d) evolution of free energy during the materials processing of UTS. (d) Adapted with permission.[10] Copyright 2025, American Chemical Society.

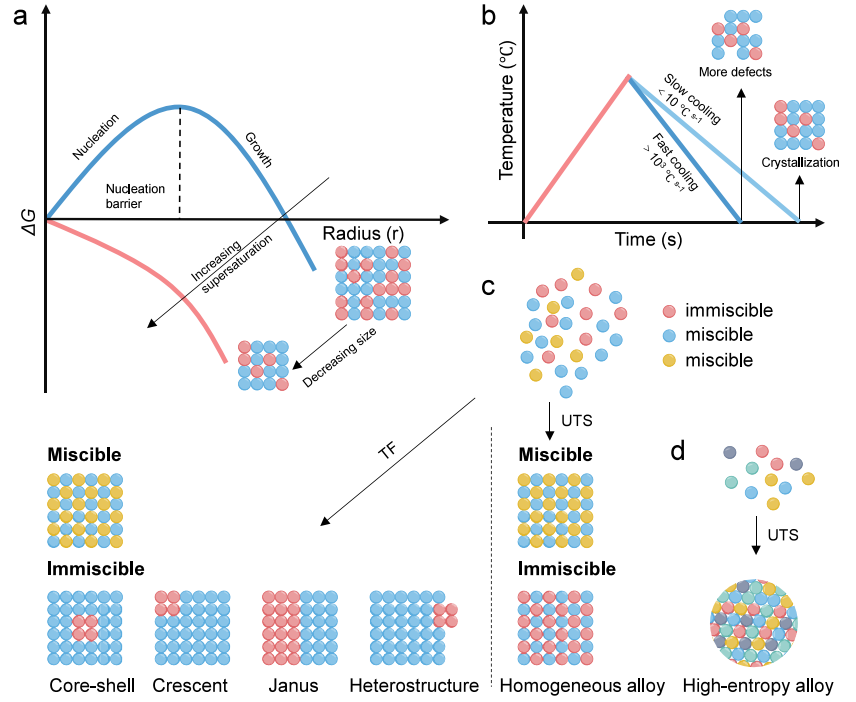

Figure 3. (a) The relation between Gibbs free energy and particle radius. (b) The relation between cooling rate and crystallization. (c) Schematic of the synthesis of bimetallic nanoparticles by TF and UTS. (d) Synthesis of a high-entropy alloy by UTS. (a) Adapted with permission.[11] Copyright 2019, American Chemical Society. (b) Adapted with permission.[12] Copyright 2022, Wiley. (c) Adapted with permission.[13] Copyright 2020, American Association for the Advancement of Science.

programmable technique of UTS can render certain precise temperature and time control by tuning the duration of electricity and the resistor's thermal conductivity or heat capacity to drive the thermochemical syntheses, on account of a resistor as a heater and electricity as an energy input in the UTS process for controlling temperature. Moreover, the heating of UTS technology is usually used to achieve objective heat treatment at a specific position in the materials, while minimizing the impact on the initial structure of materials.

2.2. Difference between Joule Heating and Carbothermal Shock. UTS typically includes Joule heating shock and carbothermal shock, which are based on the Joule heating effect. Thus, two different application types, including a Joule heating reactor and carbothermal shock reactor, are proposed. One is that the reaction precursor is directly heated by an

https://doi.org/10.1021/acsnano.5c04768
ACS Nano XXXX, XXX, XXX−XXX

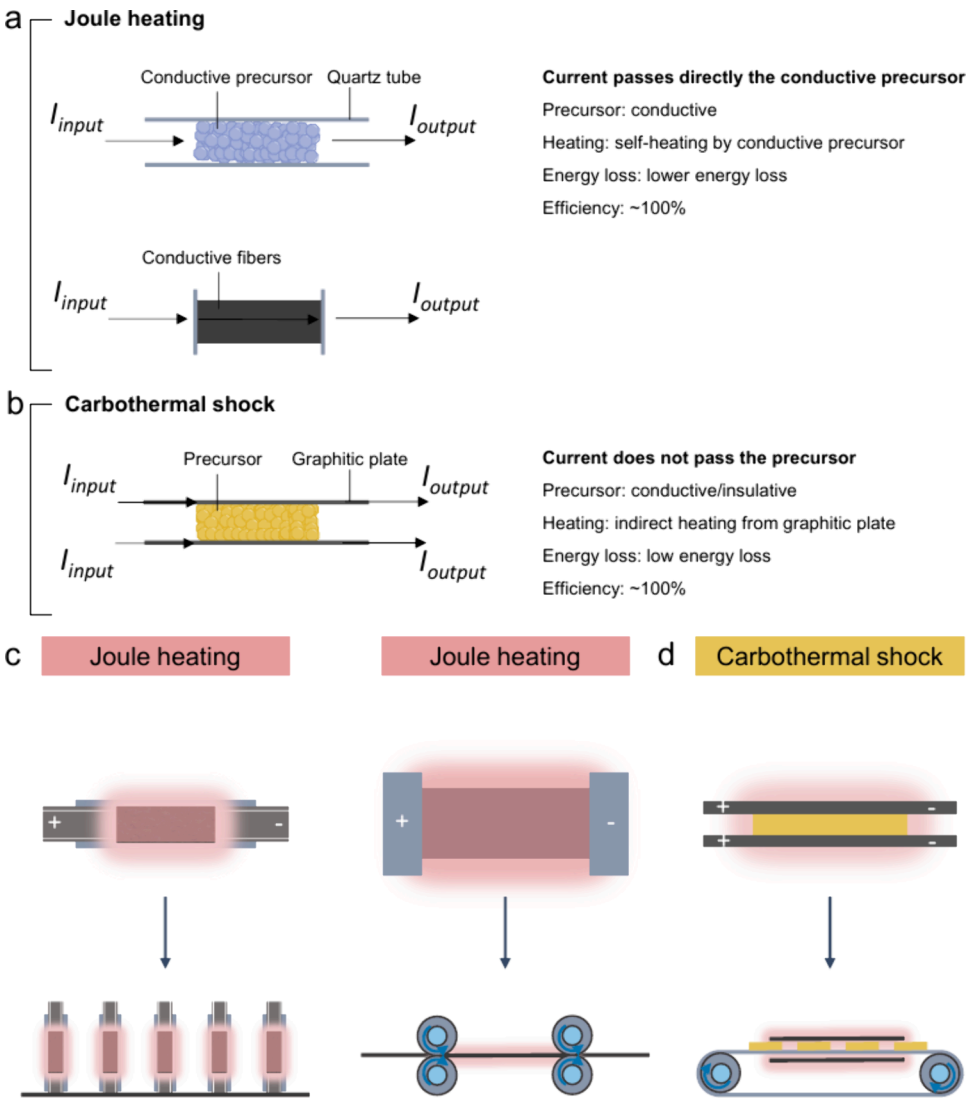

Figure 4. Schematic summarizing the types of UTS methods and their typical reactors. The characteristics of (a) Joule heating and (b) carbothermal shock. (c) Tube and film reactors of Joule heating. (d) Carbothermal shock reactor.

electric current flowing across it (Figure 4a), namely enabling the electric energy to be directly converted into thermal energy, therefore the energy loss can be reduced considerably, and close to 100% efficiency can be expected.[14−16] Due to the work condition of this technology requiring electric current to flow to the precursors and convert it into thermal energy, Joule heating reactors can only operate on highly conductive materials with superior thermal properties, which are prerequisites for desired efficiency and products and restrict the choice of reaction precursors. Quartz or ceramic tube and film reactors are designed to treat the powders and film precursors with excellent conductivity (Figure 4c), respectively. For instance, the conductive carbon-based powders including coal, biochar, and petroleum coke can be converted into graphene by these tube reactors.[17] The film reactor allows the carbon nanofibers,[18] graphene film,[19] or carbon paper/cloth[8] to act as the matrix to support the metal nanoparticles by Joule heating. For insulative powder materials like plastics and wastes, the appropriate conductive additive such as carbon black forming a mixture with insulative precursors to achieve a certain level of conductivity is a feasible strategy to afford the reaction implemented in a tube Joule heating reactor.[20]

Another approach is to solve the ultrahigh temperature heat treatment method of insulative materials without the use of conductive additives. Introducing a graphite conductive substrate (graphite paper) as the heater by Joule heating, the insulative materials loaded on the graphite substrate undergo a high-temperature heat treatment;[21,22] this process is also called carbothermal shock (Figure 4b,d). The strategies mentioned above are intermittent operations that are conducted in the experimental exploration for new materials in the laboratory, inevitably ignoring their continuous operation. To develop continuous fabrication for application in the future partial industry, a series of scale-up continuous reactors based on tube and film reactors are designed. Based on the tube reactor, a tube reactor array consisting of a number of independent tube reactors is constructed to scale up continuous fabrication. Owing to the much shorter thermal treatment time, a continuous manufacturing method of "roll to roll" is creatively proposed to realize the continuous preparation of graphene with the assistance of UTS.[23] This high-throughput system consists of three sections: film-supplying, current-feeding, and film-collecting, where the input current flows on the graphene film through the rotated graphite rollers. Another utilization

https://doi.org/10.1021/acsnano.5c04768
ACS Nano XXXX, XXX, XXX−XXX

strategy of UTS in a roll-to-roll fabrication system is that an untreated precursor can be rapidly transferred through passing face-to-face heaters. Compared with the regular UTS method, the time-efficient, low-cost, and energy-saving method through intensive UTS in tube reactor arrays and roll-to-roll preparation systems has obtained ample attention in the large-scale application prospects of thermal treatment and flexible materials.

3. APPLICATION OF ULTRAFAST THERMAL ENGINEERING IN THE DESIGN OF ENERGY MATERIALS

The performance of batteries and catalysts are related to the energy materials, including the cathode, anode, current collectors, and solid-state electrolytes in the batteries and various catalysts in the catalysis. The higher requirement of energy materials requires them to be developed rapidly to adapt to the future scene. Among diverse synthesis methods of energy materials, ultrafast thermal engineering has garnered significant attention due to its highly efficient properties, which can achieve unexpected kinetics in a shorter time. By combining carbon-based materials such as reduced graphene oxides, carbon nanofibers, carbon tubes, and porous carbon with active materials, the various metal compounds like $LiMn_2O_4$, single-atom, alloy, and even high-entropy compounds can be easily fabricated by UTS, thus dramatically enhancing the electrochemical performance.

3.1. Material Synthesis for Lithium/Sodium Batteries.

3.1.1. Cathode Materials. The cathode, as the most important component in rechargeable batteries, plays a critical role in energy density and cost. Especially a cathode with a desired crystalline structure and optimized components can offer promising prospects of boosting the electrochemical performance of batteries, which puts forward a higher requirement of the preparation process. Currently, the traditional preparation strategies of cathodes include but are not limited to melt-salt sintering, sol–gel, ion exchange, combustion, coprecipitation, and spray drying methods, which usually require complex reaction processes and long-term thermal treatment to obtain the desired crystalline structures with low heating rate and mass energy consumption. For example, melt-salt sintering through a tube furnace takes hours or even days to complete the reaction due to its low heating and cooling rate, resulting in time and energy consumption.[24] Therefore, rational and cost-efficient synthesis strategies for the preparation of cathode materials not only offer high energy density and superior cycling performance but also improve manufacturing efficiency.

Compared with traditional methods, the ultrahigh temperature shock synthesis process stands out as absolutely superior, reducing the reaction time and energy by utilizing its ultrahigh heating and cooling rate and ultrahigh temperature to achieve the synthesis of cathode materials. Furthermore, the nonequilibrium feature of ultrahigh temperature shock can compress the multistep reaction to one step. In the traditional furnace preparation process of $LiMn_2O_4$, there occurs a two-step reaction process consisting of the intermediate formation of LiO_2 and Mn_3O_4 and the final production of $LiMn_2O_4$.[25] Although the first step reaction is spontaneous over the whole temperature range, the reaction temperature of the second step must be above the critical temperature for the Gibbs free energy (ΔG) to be negative. The traditional furnaces will take a lot of time to give the required temperature of formation for $LiMn_2O_4$ because of a slow heating rate of 3 °C min^{-1}. The ultrahigh temperature shock method offers a different formation mechanism in that the reaction precursor can be directly transformed into the target products of the cathode in a short time (even seconds); namely, this method can reduce the multiple steps to one step without complicated reaction processes that often exist in conventional synthesis. According to the first-principles calculation results, ΔG always stays negative in the ultrahigh temperature shock process, indicating a spontaneous reaction and a superfast reaction kinetics (Figure 5a). In addition, the ultrahigh temperature shock

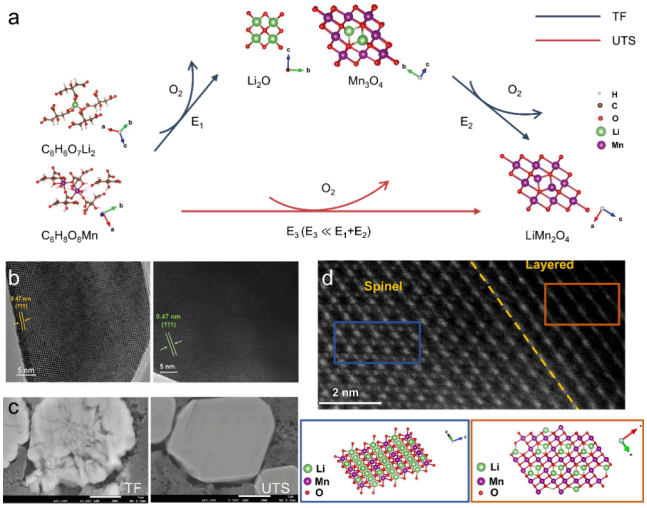

Figure 5. (a) Comparison of the reaction paths for synthesizing $LiMn_2O_4$ through TF and UTS. (b) HRTEM images of LNMO prepared by TF and UTS. (c) Cross SEM images of NCM prepared by the TF and UTS after running 200 cycles. (d) The aberration-corrected high angle annular dark-field scanning transmission electron microscopy (HAADF-STEM) image of Li_2MnO_3/$LiMn_2O_4$ heterostructure and corresponding structure. (a) Adapted with permission.[25] Copyright 2023, Wiley. (b) Reproduced with permission.[29] Copyright 2024, Springer Nature. (c) Reproduced with permission.[30] Copyright 2023, Wiley. (d) Reproduced with permission.[31] Copyright 2024, Elsevier.

method with ultrahigh heating rate and nonequilibrium reaction provides the coexistence of a high temperature environment and reduction condition constructed by high temperature, which easily causes the partial lattice oxygen loss in the metal oxides, thus inducing the generation of oxygen vacancies that are conducive to the diffusion of Li^+ and boosting of the electrochemical performance of cathode materials.[26−28] Importantly, it has been demonstrated that the universality of the UTS fabrication strategy can be applied to the synthesis versatility of cathode materials, including $LiCoO_2$, $LiFePO_4$, and Li-rich layered oxide/NiO heterostructure,[25] and they show a similar reaction mechanism that includes direct conversion in one step and production of oxygen vacancies. Indeed, the presence of certain oxygen vacancies in the cathode materials can provide a profitable metal ion diffusion environment, thus enhancing the electrochemical performance. However, the increased amount of oxygen vacancies induces the formation of a thick surface reconstruction layer, deteriorating the structural stability of the cathode and leading to inferior electrochemical cycling performance. The concentration of oxygen vacancies increases with the improved sintering temperature, the high temperature, and the long-term promise of the highly crystalline structure

https://doi.org/10.1021/acsnano.5c04768
ACS Nano XXXX, XXX, XXX−XXX

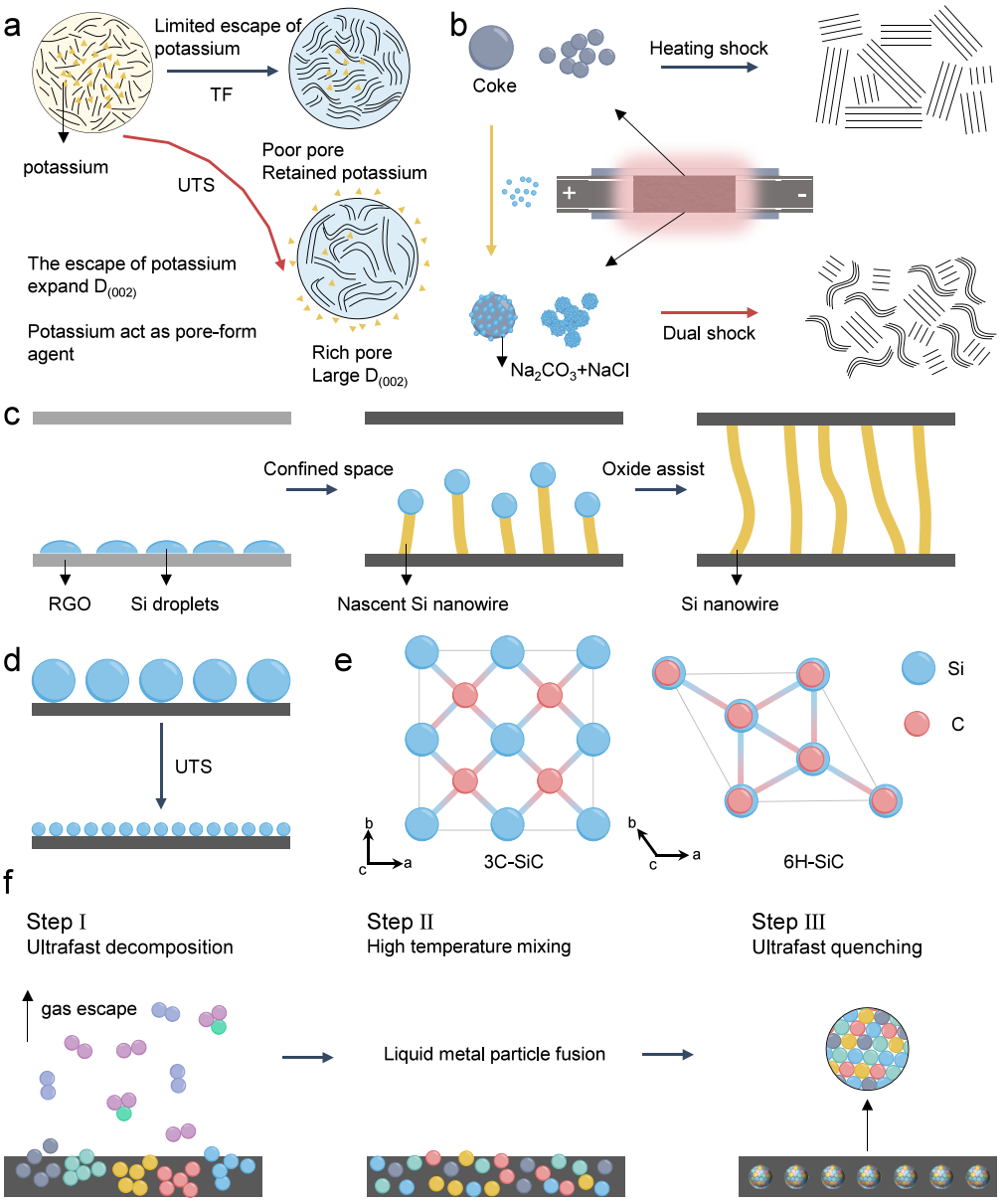

Figure 6. (a) Patterns and effects on hard carbon structural evolution induced by potassium via TF and UTS. (b) Schematic comparison of heating shock and dual shock. (c) The structure evolution of Si nanowires. (d) The illustration of particle size changes. (e) The crystal structures of 3C-SiC and 6H-SiC. (f) The structure evolution process of HEM via UTS. (a) Adapted with permission.[41] Copyright 2024, Royal Society of Chemistry. (b) Adapted with permission.[47] Copyright 2024, American Chemical Society. (c) Adapted with permission.[50] Copyright 2024, Wiley. (d) Adapted with permission.[51] Copyright 2016, American Chemical Society. (e) Adapted with permission.[52] Copyright 2024, Springer Nature. (f) Adapted with permission.[1] Copyright 2018, American Association for the Advancement of Science and adapted with permission.[53] Copyright 2022, Wiley.

that provides superior electrochemical performance. If the number of oxygen vacancies is reduced through shortening the temperature and time, the crystallinity of the cathode will decrease, destroying the electrochemical performance. As the traditional furnace takes a long time to calcinate products, it is not feasible to obtain both high crystallinity and fewer oxygen vacancies. The rapid heating rate, ultrahigh temperature, and short-time feature of UTS enable high crystallinity and fewer surface oxygen vacancies.[29] The synthesis method of the spinel $LiNi_{0.5-x}Mn_{1.5+x}O_4$ (LNMO) cathode through a traditional furnace shows higher oxygen vacancy peak intensity by X-ray photoelectron spectroscopy (XPS) than that of UTS. The quenching time of 60 s during the UTS process shows the highest ratio, indicating cathode materials with a stable structure. The high-resolution transmission electron microscopy (HRTEM) images displayed that the clear lattice fringes correspond to the interplanar distance of (111) (Figure 5b), indicating the highly crystalline structure. Due to the greater number of oxygen vacancies in the cathode by a traditional furnace, the atomic-level crystal structure shows the defective spinel structure layer with a depth of 3−4 Mn-diamond units caused by surface reconstruction, which is much thicker than that of UTS (1−2 Mn-diamond units). Therefore, fewer oxygen vacancies can decrease the thickness of the reconstruction layer, promising structure stability during electrochemical cycling.

https://doi.org/10.1021/acsnano.5c04768
ACS Nano XXXX, XXX, XXX−XXX

The larger volumetric expansion, more intergranular microcracks, and more fatal interfacial reactions of $Li(Ni_xCo_yMn_z)O_2$ (NCM, $x + y + z = 1$) during the reversible intercalation result in inferior capacity and worse safety problems, suppressing the practical application. Single-crystal cathode materials possess fewer grain boundaries, enabling the mitigation of the above problems. Of course, many single-crystal NCM cathodes have been developed through long-term higher temperature calcination, but most of them have an irregularly round morphology rather than polyhedral particles with sharp edges of a classic single-crystal structure. In short, these morphology features manifest that most of these single-crystal NCMs should be polycrystals rather than a single crystal. Additionally, the irreversible evaporation and loss of Li during the long-term higher temperature sintering varies from the surface to the internal part. Therefore, it is feasible to shorten the sintering time to obtain the desired single-crystal cathode materials. Pulse UTS imported into the traditional sintering process was developed for the preparation of single-crystal NCM, which only takes 60 s to reach 1040 °C in the UTS step to obtain well-defined octahedral particles.[30] The size and crystallinity of particles increase with increasing temperature, but the highest temperature (1060 °C) condition shows the lowest initial Coulombic efficiency (ICE) due to the heavy Li/Ni ratio. Compared to traditional furnaces, there is an absence of internal void holes and nanoslits in the core and shell of single crystal NCM. There exist increased microcracks in the NCM by a traditional furnace after 200 cycles, while single-crystal NCM still remains smooth without any microcracks (Figure 5c), indicating its outstanding structure stability during long-term electrochemical cycling. In addition, the reduced interfacial reaction with the electrolyte leads to a thinner cathode electrolyte interface layer, thus endowing the most stable cycling performance.

Besides the synthesis of single-phase cathode materials through the UTS strategy, rationally adjusting the temperature, time, composition, and sintering atmosphere can give heterostructure materials that integrate the merits of a biphasic structure, endowing an enhanced structure stability under the synergistic effect of different components. Additionally, the forming heterointerface can improve the charge and metal ion transfer to boost the electrochemical performance. For example, the electrochemically inert layered Li_2MnO_3 and active spinel $LiMn_2O_4$ phases form a good heterostructure in seconds through UTS methods (Figure 5d).[31] In this process, excess Li (Li/Mn = 1.09/1.91), ultrafast heating rate, and short reaction time play critical roles in the construction of the layered/spinel heterostructure, while only $LiMn_2O_4$ and Li_2MnO_3 were obtained with a reduced amount of Li (Li/Mn = 1:2) and using a traditional furnace, respectively. Benefiting from the heterostructure, $Li_2MnO_3/LiMn_2O_4$ shows negligible voltage polarization and an outstanding cycling performance. In this heterostructure, Li_2MnO_3 can effectively restrain the Jahn−Teller effect of MnO_6 in $LiMn_2O_4$, thus improving the structure stability. Lithium-rich cation-disordered rock salt (DRX) oxides possess promising prospects, but Li-rich DRX oxides consist of an amount of metastable state Li−O−Li ligands, which can be susceptibly inevitably oxidized and result in metal dissolution and phase separation, thus causing an undesired electrochemical performance. UTS methods were introduced to synthesize DRX oxides to address the existing problems.[32] The variety of transition metals in DRX oxides can easily be synthesized rather than traditional thermal treatment and ball-milling and extended from binary ($Li_{1.2}Co_{0.4}Nb_{0.4}O_2$) to the senary ($Li_{1.2}Co_{0.1}Mn_{0.1}Mn_{0.2}Cr_{0.1}Ti_{0.2}Nb_{0.2}O_{0.2}$). Moreover, benefiting from the rapid heating process of UTS, a more compact and highly uniform $NaCaPO_4$ coated on the surface $NaNi_{1/3}Fe_{1/3}Mn_{1/3}O_2$ prevented nickel migration and enhanced the structure stability, outpacing the electrochemical performance of cathodes prepared by TF.[33]

3.1.2. Anode Materials. During the preparation of anodes for second batteries, the UTS method also stands out with significant and unique merits. Especially in the exploration of carbon-based anodes, the ultrahigh temperature and fast reaction time of UTS provides many possibilities for the degree of carbonization, electrical conductivity, structure, and surface area, which affect the ion diffusion kinetics, capacity, ICE, and stability of batteries.[34−37] Due to the properties of the UTS method, some carbon derived from biomass can inherit the original feature of biomass that possesses an open and interconnected pore structure.[38,39] As a breakthrough, in 2017, the stem of switchgrass was first carbonized into hard carbon under an ultrahigh temperature (2050 °C) by the UTS method.[40] The obtained hard carbon exhibited a porosity similar to that of the switchgrass precursor, higher electrical conductivity, a more ordered pseudographite structure, and decreased surface area, facilitating electron and ion transport for excellent Na ion storage performance. Additionally, the shorter time and ultrahigh temperature of UTS could not only promote the escape of inherent ash elements (like K) in biomass for forming the abundant pore but also avoid the overgraphitization of biomass-derived hard carbon to enhance the sodium storage performance,[41,42] addressing the problems including limited escape of ash and overgraphitization under high temperature in the traditional tube furnace (Figure 6a). For the carbonization of carbon sources with aromatic structures, the carbon layers tend to suffer orderly stacking and graphitization because of the complex changes in the precursor, causing an inferior sodium performance. The higher heating rate is regarded as an efficient strategy to tackle this problem; however, the traditional high-temperature furnace is unsatisfactory to achieve such a high rate. The UTS process not only satisfies the requirement of heating rate but also can generate the Joule heat during the resistance surrounding the conductive pathways along the interconnected aromatic layers, which can alleviate the carbon layer stacking.[43] Additionally, the more enclosed pores can be formed by fusing the open carbon edges under the effect of Joule heating.[2,35,43] On prolonging the heating time, the graphitized layers also increased from 30 to 42.5 nm.[44] But, suitable graphitized layer thickness is important to enhance the electrochemical performance. The formed graphitized layer (30 nm) encapsulated carbon nanofiber heterostructure not only reduced side reactions between electrolyte and electrode but also enhanced the reversibility of Li^+/metal storage. Uniform lithophilic Ag nanoparticles decorating carbon nanofibers by UTS can modulate the interface chemistry to further improve the electrochemical performance.[45] Notably, the ordered graphite structure of carbon layers also significantly improves with the increased number of UTS cycles.[43] However, the selection of the number of UTS cycles is determined by the performance of the sodium ion battery. The anthracite coal derived hard carbon after three UTS processes shows moderate carbon layer thickness, closed pores, and larger interlayer spacing, exhibiting more excellent sodium storage

https://doi.org/10.1021/acsnano.5c04768
ACS Nano XXXX, XXX, XXX−XXX

performance. Nevertheless, the graphite anode obtained through UTS usually shows turbostratic arranged graphene layers, which prolong the in-plane ordered ranges and diffusion path of Li^+, further displaying unsatisfactory capacities.[2,46] The introduction of an activator and the combination of the UTS process with ball-milling that were adopted to disrupt the long-range order structure of graphite have been demonstrated to address these issues and improve the anode capacities.[47−49] For instance, activators, such as Na_2CO_3, NaCl, K_2CO_3, and KCl, can be decomposed into CO_2 gas and Na vapor at ultrahigh temperature, thus generating a pressure for mechanical shock to the graphite (Figure 6b).[47] Under the synergetic effect of ultrahigh temperature shock and mechanical shock (dual-shock), the carbon can be thermodynamically graphited and bent, converting into a distinctive hybrid structure involving ordered graphite and disordered amorphous carbon, which improves the amount of lithium storage sites and enhanced charge transfer, respectively.

To develop high-energy-density lithium-ion batteries, an anode involving Si with higher theoretical specific capacity is regarded as the alternative electrode. However, Si anodes suffer from ample volume changes during the charge−discharge process, deteriorating the electrochemical performance and stability and impeding their development and application. Rational design of structures, such as nanoparticles and nanowires, can efficiently solve this issue. However, these nanostructures usually require harsh conditions that can be achieved, and the selection of reaction conditions or approaches is important to prepare the favorable structure. For example, the construction of a large-gradient thermal atmosphere is extremely necessary to drive the transformation of Si powders into Si nanowires without any catalysts.[50] In this process, reduced graphene oxide (RGO), with excellent conductivity, generates ultrahigh temperature (∼2100 K, 10 ms) by Joule heating for large-gradient thermal fields. The Si powders in the RGO layers undergo the formation of droplets and growth into nanowires in the one-dimensional directions (Figure 6c). Note that this approach can be applied to any ratio of Si and graphene (GO) without any fine condition control for obtaining the expected nanowire structure; there is a slight difference in the diameters of the nanowires. As anodes of LIBs, the Si nanowires/RGO exhibit a superior initial Coulombic efficiency (89.5%) and long-stability (2381.7 mAh g^{-1} at 1 A g^{-1}, 500 cycles) at a high Si content of 76%, which are attributed to the nanowire structure mitigating the variation of volume. Moreover, due to the airflow on the surface of the RGO film, the Si nanoparticles form and are uniformly distributed on the upper surface of the RGO, also confirming that the key role of confined space by the RGO significantly affects the formation of Si nanowires. According to this phenomenon, the conversion of Si/Al/Sn particle size from micrometers to nanometers and uniform dispersion in the graphene matrix by the UTS approach gained more attention.[51,54] Before the UTS process, the metal particles with GO mixture precursor should be pretreated by reduction at low temperature in an inert gas atmosphere, ensuring the generation of RGO from GO. This is because the current needs to pass through the conductive matrix, which is suspended RGO film in these systems. More importantly, the fine-tuning of the heating temperature, hold time, and ratio in the UTS process allows the preparation of different sizes and phases of nanoparticles embedded into the RGO matrix (Figure 6d). The nanoparticle size of Sn increases to approximately 50 nm with the prolonged reaction time from 30 s to 1 h. However, the new phases of SiC could be synthesized while the temperature increases from 1800 to 1900 K. These results further reveal the key role of temperature in fabricating desired materials.[51] According to these reports, the selective preparation with different phases, 3C-SiC and 6H-SiC anodes, has been successfully achieved by tuning the reaction temperature of UTS (Figure 6e).[52] Density functional theory (DFT) calculation results elucidate the content of Si vacancies acting as a key role in the formation of different phases of SiC. Consequently, the precursors transform into 3C-SiC with a single flash at an input voltage of 100 V, which generates a low content of Si vacancies. While the input voltage and flash time increase to 150 V and 10 times, respectively, more Si vacancy generation induces the formation of 6H-SiC, which is more thermodynamically stable. The 3C-SiC and 6H-SiC anodes both exhibit a stable capacity. However, the 3C-SiC anode shows superior reversible capacity over the 6H-SiC anode, which is attributed from the higher electron transfer and enhanced Li^+ diffusion kinetics of the 3C-SiC For the traditional furnace thermal reduction, the longer reaction time and lower heating and cooling rates restrict the SiC phase control. Therefore, it is important and helpful to control the crystal phase of anodes to obtain ideal performance by fine control of the experimental conditions during the ultrafast heating and cooling rate of the UTS process. And the conventional carbothermal reduction processes, consuming a longer time, restrict the selective synthesis of SiC.

Recently, high-entropy materials (HEMs) have featured complex element composition and tunable properties, attracting intense attention in the application of LIB anodes.[55] However, the synthesis process remains a formidable challenge; the preparation condition requiring a high-temperature and rapid cooling process protects the effect of uniform mixing of diverse elements into single-phase HEM from the phase separation taking place during the prolonged quenching process.[56] In past research, most of the fabrication approaches are based on a traditional electrical furnace, which are time- and energy-consuming, taking up to several hours to achieve the desired temperature with a lower heating and cooling rate. The ultrafast heating and cooling rate of the UTS process can accelerate the development of HEMs, offering sufficient activation energy for the formation of a stable, high-purity crystalline phase. As shown in Figure 6f, the UTS methods for forming HEMs include three steps involving the decomposition and mixing of various metal salts under fast and ultrahigh temperatures and the formation of HEM with a single-phase structure under an ultrafast cooling rate. Thus, the rational control of UTS condition parameters (temperature, holding time, heating/cooling rate, and so on) can be widely applied to prepare various HEMs with the expected composition, size, and phase. Recently, a series of high-entropy oxides (HEOs) were successfully prepared through UTS methods in 3−10 s with a holding temperature of ∼1060 °C,[57] including (MgCoNiCuZn)O, (MgCoNiMnZn)O, $(FeCoNiCrMn)_3O_4$, and so on, while the impurity existing in the (MgCoNiCuZn)O is also tackled through an ultrafast heating and quenching process. As an anode material of LIBs, (MgCoNiCuZn)O exhibits a high capacity of ∼150 mAh g^{-1} at 10 A g^{-1} and cycle stability over 2600 cycles. Subsequently, the preparation of $(Mg_{0.2}Co_{0.2}Ni_{0.2}Cu_{0.2}Zn_{0.2})Fe_2O_4$ by tuning the reaction temperature and time of UTS processes confirms again that the UTS method is a feasible strategy for fast and

https://doi.org/10.1021/acsnano.5c04768
ACS Nano XXXX, XXX, XXX−XXX

efficient synthesis of various HEMs in a short time, which is shorter by more 20,000 times than conventional synthesis approaches.[58] Meanwhile, $(Mg_{0.2}Co_{0.2}Ni_{0.2}Cu_{0.2}Zn_{0.2})Fe_2O_4$ as an anode displays a superior reversible capacity and long-term cycle stability in the electrochemical test of LIBs.

3.1.3. Current Collectors. With the improvement of energy density and long-term durability, carbon-based current collectors, including carbon nanotubes, graphene, and flexible graphite foils,[59−62] have attracted much attention for electrochemical energy storage and electrocatalysis applications owing to their light weight, flexibility, high conduction, and anticorrosion in harsh chemical environments. However, the poor physical contacts between nanostructures cause relatively high electrical conductivity, resulting in an unsatisfactory electrochemical performance. Besides, it is difficult to open and reform covalent carbon bonds between adjacent carbons because of the inertness and high bond energy of C−C. Of course, high-energy radiation or high-pressure methods can achieve the opening and reforming of covalent carbon bonds.[63−67] These strategies can not only destroy the original physical structures and generate a lot of undesired defects in carbon materials but also restrict scalability due to the special equipment required. Thus, previous reports proposed the application of the UTS approach to optimize carbon-based current collectors.

Benefiting from the fast heating rate and ultrahigh temperature of UTS technology, a similar high energy can be easily obtained because of the higher resistance at the physical contact point between carbon materials, which facilitates the transformation of covalent carbon bonds. Under the high-temperature environment (>2500 K) and ultrafast heating rate (~200 K min^{-1}), polyacrylonitrile (PAN) based carbon nanofibers can be further carbonized and welded together as adjacent nanofibers with graphite bonds, thus forming a 3D covalently bonded carbon interlocked framework which had been proven theoretically but not experimentally (Figure 7a).[68,69] The fusion between adjacent nanofibers can be speculated as collisions between electrons and atoms in the nanofibers inducing excessive vibrations of the carbon layers during the UTS process. And high temperature also further improves the crystalline degree of carbon. With the optimization of structure and graphitization, welded carbon nanofibers films show a superior electrical conductivity of 380 S cm^{-1} with a sheet resistance of 1.75 Ω sq^{-1} and tensile strength (3.86 MPa) and toughness (20.65 kJ cm^{-3}) compared to the pristine carbon nanofibers (0.0133 S cm^{-1}, 18400 Ω sq^{-1}, 0.31 MPa, and 1.265 kJ cm^{-3}, respectively). The direct welding of PAN can be successfully achieved by applying UTS technology, which is related to the amorphous structure of starting materials. With the activation and removal of H and N in the PAN at high temperature, Bergman cyclization between adjacent nanofibers occurs and new C−C covalent bonds are constructed to fuse the amorphous structure carbon nanofibers. Highly crystalline carbon materials such as carbon nanotubes (CNTs) did not easily form a 3D continuous network through directly welding adjacent CNTs by UTS, as high temperature generated at the junction did not deform the stable C−C bonds present.[70] Thus, the novel "epitaxial welding" approach by UTS is proposed to engineer CNTs into interconnected 3D structures (Figure 7b).[71] Solution-based PAN was conformally coated along the outer surface of CNTs to physically mix CNTs into a framework, and the epitaxial growth of the PAN was *in situ* graphitized into highly

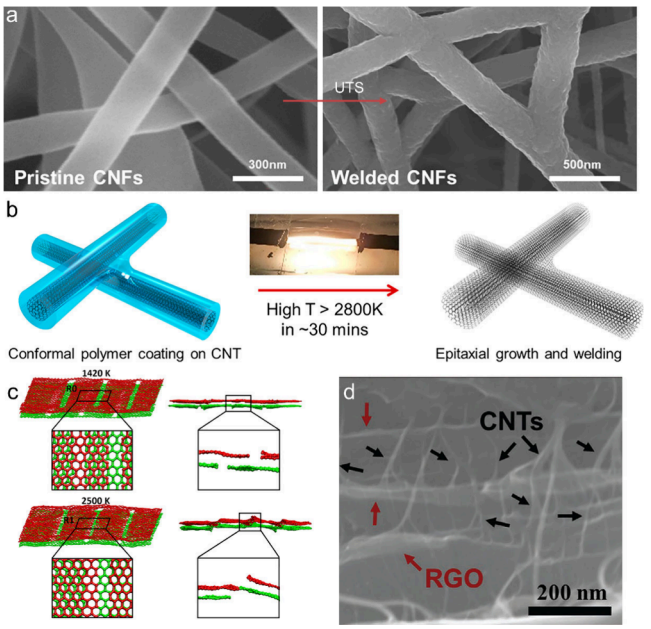

Figure 7. (a) SEM images of CNFs before and after UTS treatment. (b) Illustration of epitaxial growth and welding of CNT. (c) Molecular dynamics simulations of the formation of interlayer bridging bonds. (d) SEM image of RGO-CNTs. (a) Reproduced with permission.[68] Copyright 2016, American Chemical Society. (b) Reproduced with permission.[71] Copyright 2018, American Chemical Society. (c) Reproduced with permission.[72] Copyright 2016, American Chemical Society. (d) Reproduced with permission.[73] Copyright 2020, Wiley.

crystalline carbon at high temperature (>2800 K, overall ~30 min) by Joule heating, effectively welding adjacent CNTs together. The obtained CNT 3D networks exhibit high electrical conductivity and mechanical strength. Notably, the energy consumption of UTS is less than 20 W compared to traditional furnaces, suggesting its energy efficiency.

The successful practice of welding 1D carbon materials suggests the key role of UTS technology in opening and reforming the covalent carbon bonds, which can improve the electronic conductivity of 1D carbon materials. A lot of graphene nanosheets as a 2D structure were also widely used in the current collector. However, the sheet−sheet junction resistance of graphene limits the conductivity to 100 S cm^{-1}, and pristine graphene through the reduction of graphene oxide (GO) remains a grand challenge because of the impendent of defects and functional groups. The self-healing and reforming provided by UTS technology can solve these issues efficiently. The ultrahigh temperature enhances the reactivity of carbon atoms with dangling bonds in graphene oxides. With the temperature increasing from 300 to 2500 K, the interlayer sliding between the top and bottom graphene layers further facilitates the construction of bridging bonds when the line defects come close to each other (Figure 7c).[72] After the treatment with UTS, the formation of cross-links between adjacent reduced graphene oxides at defects contributed to the construction of highly dense films and improved the electrical conductivity. Besides, the reduction of a GO-CNT mixture by UTS at 2936 K within less than 1 min also successfully fabricated a high electrical conductivity reduced graphene oxide (RGO)-CNT current collector (Figure 7d), which shows a 6 orders of magnitude increase to 2750 S cm^{-1} and superior mechanical ability.[73]

https://doi.org/10.1021/acsnano.5c04768
ACS Nano XXXX, XXX, XXX−XXX

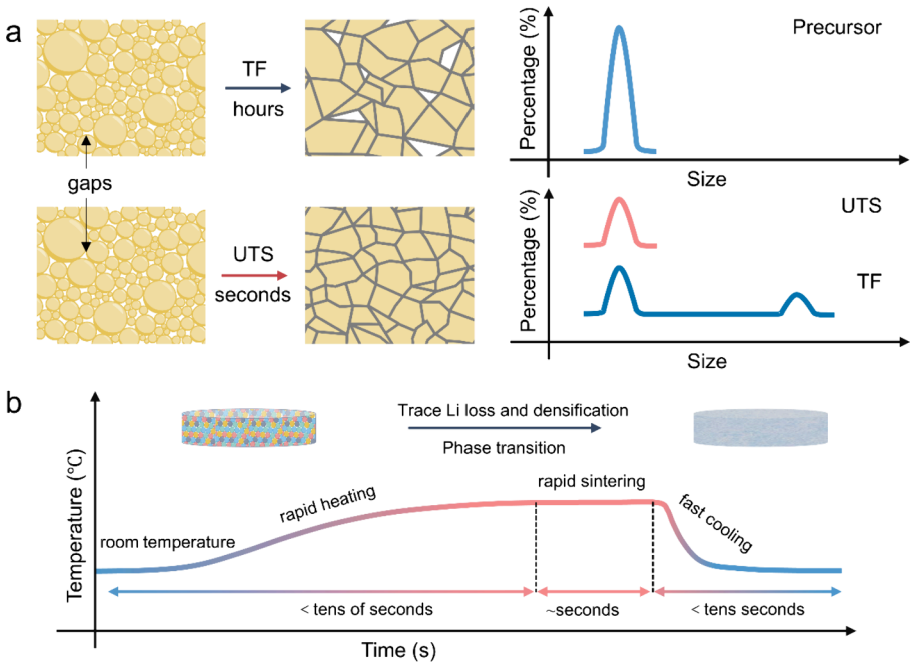

Figure 8. (a) Schematic comparison of the particle size distributions of ceramic solid-state electrolyte preparation by TF and UTS. (b) A typical heating temperature profile as a function of time. (a) Adapted with permission.[76] Copyright 2021, American Chemical Society. Reproduced with permission.[77] Copyright 2021, Elsevier and reproduced with permission.[83] Copyright 2024, Wiley. (b) Adapted with permission.[78] Copyright 2020, Wiley and reproduced with permission.[79] Copyright 2018, Elsevier.

3.1.4. Solid-State Electrolytes. In the development of ceramic-based solid-state electrolytes (SSEs), the sintering technology has become a major approach to achieving higher ion conductivity and density, which are critical for improving solid-state battery (SSB) electrochemical performance.[74,75] The conventional sintering process usually provides a temperature of up to ~1600 °C with low heating rates, thus resulting in Li loss, side reactions, wide particle size, and loose structure due to the long-term low-temperature process time (Figure 8a).[76,77] Especially, the high thermal stability ceramic-based SSEs require a much higher sintering temperature, which the traditional furnace usually spends several hours to achieve, and the UTS strategy by carbothermal shock can provide uniform high-temperature conditions to rapidly heat the SSEs through radiation and conduction. To avoid severe Li loss and side reactions, reducing sintering time becomes an efficient strategy to prevent volatile evaporation and undesirable phase diffusion (Figure 8b).[76,78,79] Compared to traditional thermal technology, the UTS can rapidly heat the objective to high temperature (up to 3000 K) in milliseconds, which provides rapid kinetics, additional chemical driving force, and ultrahigh heating rates to enhance the densification.[22,77−80] Although the densification and Li-evaporation rate both increase with temperature, the garnet SSE densification rate increases more rapidly than the evaporation rate, thus resulting in less Li loss in the shorter sintering time and a high-density structure.[22,79] The fine control of sintering temperature can efficiently balance between Li loss and a dense microstructure. When the temperature reached 1100 °C within 5 s, the $Li_{6.5}La_3Zr_{1.5}Ta_{0.5}O_{12}$ (LLZTO) with incompletely desirable dense microstructure showed less Li loss, whereas the obtained dense membrane structure exhibited severe Li loss at 1500 °C.[81] Consequently, a rational temperature region between 1000 and 1500 °C is usually selected to fabricate and investigate the Li loss and grain growth for high ion conductivity and dense structure.[75,77,79,82]

Besides, the traditional furnace usually exists in the long-term low-temperature region, where surface diffusion occupying the domination leads to coarsening and neck growth without densification. UTS, with fast heating rates and high temperature, not only bypasses the low-temperature region but also offers a desirable high-temperature environment for densification, which is attractive compared with conventional sintering approaches. The efficient grain growth and bulk diffusion can dominate at high temperatures by UTS and lead to fast densification.[22,77,82] The removal of numerous gaps, voids, and pinholes between the grains at high temperatures was attributed to the grain growth to form a dense structure without additional filler. With prolonged sintering time under high temperatures, the grain boundaries gradually grew with the driving force of surface energy, and the grain size increased to a larger size, thus filling the gaps and forming a denser microstructure. However, the longer sintering caused excessive grain growth, inducing the disappearance of grain boundaries and the formation of surrounding smaller grains, which created new voids and gaps. Meanwhile, the Li loss further increased, and relative density decreased.[22,77] It is noteworthy that a high temperature and fast heating rate can also address the unattainable introduction of sintering aids and Li compensation by traditional furnaces. Due to the high volatility and low melting point of desirable sintering aids like Li_3N and LiOH, long-term conventional approaches cannot incorporate aids without severe Li loss and cause a porous structure.[76,80] More importantly, the rapid synthesis property of UTS can validate the computational prediction during the high-performance SSE synthesis,[78] where high-throughput screening provides vast opportunities for material development. The significant increases of calculated configurated entropy with multiple elements at the Zr site in garnets, ranging from 1 to 10,

https://doi.org/10.1021/acsnano.5c04768
ACS Nano XXXX, XXX, XXX−XXX

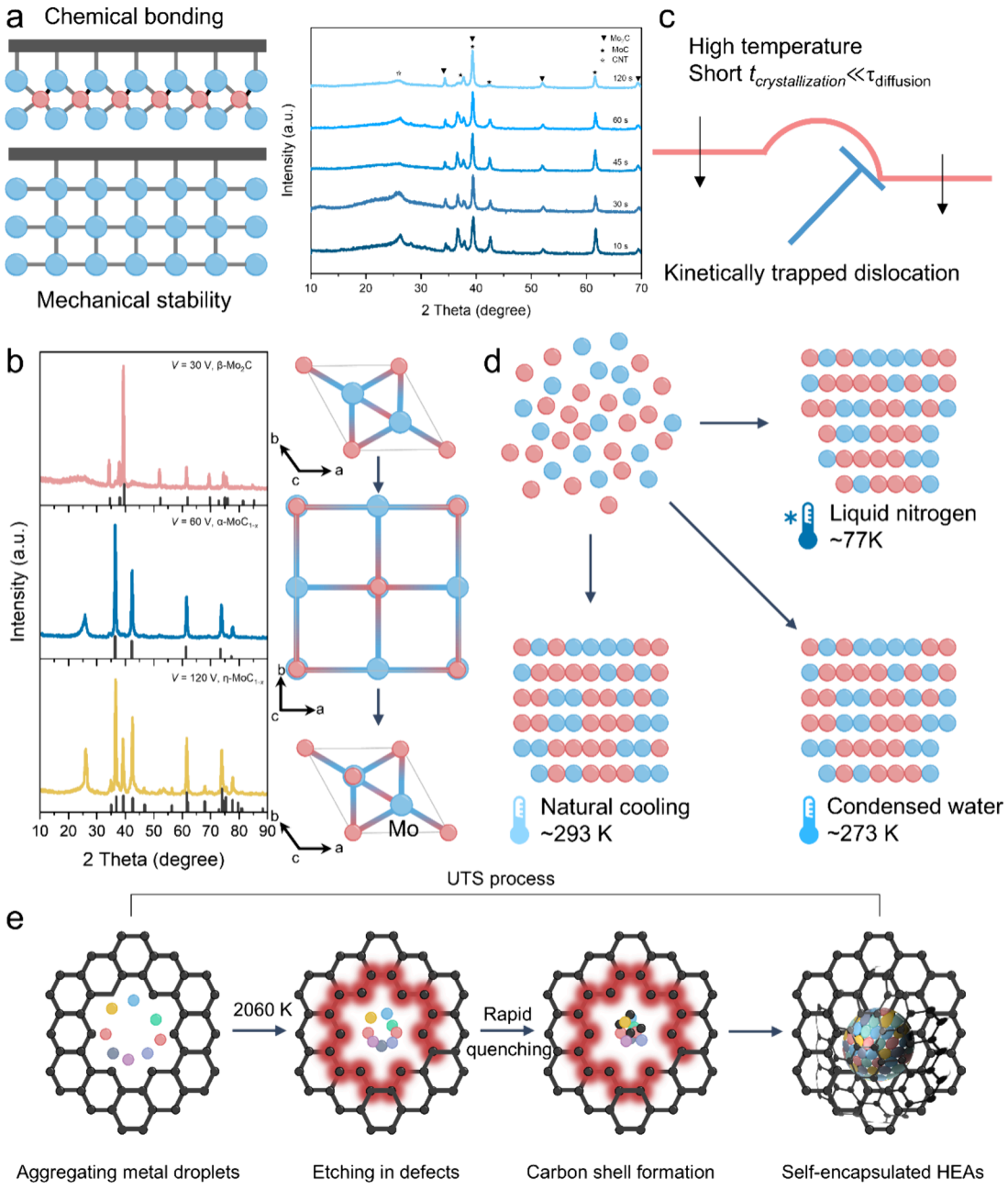

Figure 9. (a) Schematic illustration of enhancing structure and XRD patterns at different times. (b) XRD patterns and crystal structure of different phases. (c) An illustration of dislocations. (d) The crystal structure changes under different extreme quenching processes. (e) Schematic illustration of the self-encapsulation of HEAs driven by defect-driven surface engineering. (a) Adapted with permission.[88] Copyright 2022, Springer Nature. (b) Adapted with permission.[89] Copyright 2022, Springer Nature. (c) Adapted with permission.[96] Copyright 2024, Wiley. (d) Reproduced with permission.[97] Copyright 2024, Wiley; reproduced with permission.[98] Copyright 2022, Wiley. (e) Reproduced with permission.[99] Copyright 2024, Wiley.

indicate that solid solutions occupy the "high-entropy region".[84] To rapidly demonstrate the effect of high-entropy cubic garnets, traditional "trial-and-error" strategies cannot satisfy the tremendous exploration space. Through the UTS approach, a series of high-entropy garnets were successfully synthesized, and the entropy-stabilization effect, configuration entropy increasing could result in the phase transformation from garnet to pure cubic, was discovered.

3.2. Materials Synthesis for Energy Conversion Catalysts. In addition to the energy storage represented by batteries, heterogeneous catalysis has been considered a promising approach for energy conversion, such as water splitting involving the hydrogen evolution reaction (HER) and oxygen evolution reaction (OER), oxygen reduction reaction (ORR), and CO_2 reduction reaction (CO_2RR) and nitrogen reduction reaction. During these energy conversion processes, catalysts with high activity and stability play a critical role in improving performance and promoting their development. Although platinum- and rhodium-based catalysts exhibit exceptional catalyst activity,[85−87] their high prices cause huge costs. Developing catalysts with the same performance as conventional noble metal catalysts from non-noble metals or lowering the content of noble metals has become the main target for reducing cost and increasing efficiency. Therefore,

https://doi.org/10.1021/acsnano.5c04768
ACS Nano XXXX, XXX, XXX−XXX

extensive efforts have been devoted to designing and fabricating highly active catalysts by various synthesis strategies, including solvothermal means and calcination, which can be further improved by adjusting the size, distribution, electronic structure, and specific active surface area. As reported, the UTS technique, an effective synthesis process for the high distribution, ultrafine size, and large surface area of nanoparticles, is a versatile but simple method that leads to a significant impact on the development and fabrication of new catalysts.

3.2.1. Hydrogen Evolution Reaction Catalysts. Hydrogen energy, as an important green energy with a high energy density, is considered a promising alternative to fossil fuel. Electrocatalytic water-splitting has been regarded as an effective approach for producing hydrogen, where various HER catalysts such as Pt, Ru, Ir, Mo, Fe, and Ni were explored through the UTS strategy to enhance the HER kinetics. Mo-based electrocatalysts, such as Mo carbides and oxides, exhibit application in the future in HER due to their earth-abundant, outstanding electrochemical properties. However, the traditional methods by a tube furnace for preparation of Mo-based catalysts include energy and time consumption and inevitably cause agglomeration or coke surface due to slow reaction kinetics, which is detrimental to improving HER performance. The instantaneous heating properties of UTS can efficiently solve the above issues; the Mo_2C/MoC nanoparticles uniformly distributed on CNT were derived from a mixture of ammonium molybdate, glucose, and urea by a UTS method,[88] and the effect of rapid high temperature enhanced the strong chemical bonds between the CNT matrix and Mo, which avoids the peeling off of nanoparticles and ensures the stability in a long-term HER process (Figure 9a). Besides, the ratio of α-MoC and β-Mo_2C could be tuned by applying different temperatures or heating times, where α-MoC converted to β-Mo_2C at high temperatures or a long time. The heterointerface between α-MoC and β-Mo_2C was considered as the main contribution to the HER activity; thus, ultrafine control of reaction temperature or time became crucial for the preparation of high-performance catalysts. As a result, Mo_2C/MoC loaded on CNT catalysts only required an overpotential of 233 mV to achieve 1000 mA cm^{-2} at 1 M KOH and could stably work 14 days at 1000 mA cm^{-2}. When the precursor included $MoCl_3$ and carbon black, the similar phase conversion between α-MoC_{1-x} and β-Mo_2C also occurred at high temperatures by high voltage discharging.[89] With the increase in temperature from 839 K (30 V) to 1468 K (60 V) and 3242 K (120 V), β-Mo_2C, α-MoC_{1-x}, and η-MoC_{1-x} were finely synthesized (Figure 9b), respectively. The faster nucleation kinetics at high temperatures also promoted the formation of the smallest particle size of η-MoC_{1-x}. Notably, this phase conversion pathway where β-Mo_2C transformed to α-MoC_{1-x} and α-MoC_{1-x} was further converted to η-MoC_{1-x} is different from previous reports.[88,90] DFT results indicated that the carbon vacancies may serve as the main driving factor for this distinct phase transition process. Due to the enhanced metallicity of β-Mo_2C, it exhibited HER performance superior to that of others, suggesting significant phase-dependent HER activity.

Rich uncoordinated Mo^{4+} sites in catalysts are conducive to improving the HER electrocatalytic performance. The prolonged heating time of traditional methods inevitably leads to the oxidation of Mo^{4+}. Thus, the rapid UTS technique was conducted to avoid excess oxidation of Mo for synthesizing HER catalysts. A series of MoO_x/NF-based species were successfully synthesized.[91−93] $Co_2Mo_3O_8$/MoO_2/NF exhibited rich uncoordinated Mo^{4+} sites and lattice dislocation by the UTS method, resulting in strong Mo−O bonds and electron arrangement.[94] With a double effect, the obtained catalysts showed excellent electrocatalytic activity and a low Tafel slope. Impressively, UTS and CVD were both conducted to prepare the same phase composition of NiFe alloy/MoO_2/NF.[95] However, UTS only consumed 0.021 kWh energy and took 180 s; the energy consumption and time of UTS are far lower than those of CVD. Not only was MoO_2/NF with Mo^{4+} sites obtained, but also the rapid heating/cooling process induced the formation of face-centered cubic phase FeNi alloy and a shorter bond length (2.50 Å) of Fe−Ni, further improving the electrical conductivity and amounts of O defects, leading to HER electrochemical performance (20 mV@10 mA cm^{-2}) superior to that of FeNi alloy synthesized by CVD exhibiting body-centered tetragonal phase FeNi with a length of 2.53 Å.

Strain engineering, such as dislocations or grain boundaries, can optimize the electronic structure of catalysts for enhancing electrocatalytic reactions. It is found that the nonequilibrium process of UTS could induce various defects due to the ultrafast quenching (Figure 9c). Meanwhile, the different atomic radii of Ir and Ni further promoted the generation of dislocations in the millisecond-class heating treatment process.[96] IrNi nanoparticles with abundant dislocation distributed on CNT displayed better HER activity with a 17 mV overpotential at 10 mA cm^{-2}. To improve the thermal difference condition, in addition to increasing the heating temperature to a higher range, improving the cooling rate and reducing the final temperature are effective approaches (Figure 9d). Further accelerating the cooling rate was achieved by condensed water flowing through the synthesis chamber, resulting in a great temperature gradient experienced by the Ir nanoparticles. The generation of thermal stress could induce the vacancies to collapse to produce dislocations within the nanoparticles; there were rich Frank partial dislocations in the Ir nanoparticles.[97] Compared to the standard Ir PDF, the Ir/C catalysts exhibited a 4% compression of the (111) plane. Benefiting from the 4% strain effect, the Ir−H bonds were weakened to improve the Tafel step. The Frank partial dislocations also may slightly increase the electrochemically active area to 90 m^2 g^{-1} over that of traditional furnace sintering, thus ensuring the exposure of active sites. Overall, the Ir/C with rich dislocations can show outstanding mass activity in an acidic solution, which achieved 6.64 A mg^{-1} at 50 mV. When the UTS procedure occurred in the extreme environment created by liquid nitrogen, a huge temperature gradient caused by ultralow temperature (∼77 K) generated thermal stress.[98] Meanwhile, structural stress formed on the joints between different crystallized Pt atoms. These two stresses have a significant effect on the Pt atomic structure, resulting in plastic deformation and further triggering of dislocations. Notably, the formation of a dislocation began to occur at the cooling stage. The strain caused by the dislocation could downshift the d-band center, which led to a weakened adsorption between the active sites and H* to enhance the HER performance.

Because a metal salt can be decomposed and redistributed on the carbon matrix under high temperatures, high-density ultrafine metal nanoparticles uniformly distributed on the carbon support were developed by UTS for HER. The typical

https://doi.org/10.1021/acsnano.5c04768
ACS Nano XXXX, XXX, XXX−XXX

synthesis procedure consisted of a carbon matrix loaded metal salt precursor by dip coating and then UTS heating treatment.[18,100,101] According to this method, NiFe alloy nanoparticles encapsulated by a thinner-graphene layer in the carbonized wood were proved to be prepared successfully.[102] The obtained N-C-NiFe nanoparticles exhibited a smaller particle size of 22.5 nm and thinner graphene layers (1−4 layers), while NiFe nanoparticles prepared by a traditional furnace possessed 175 nm of nanoparticles and 9 layers of graphene. The results demonstrated that the rapid quenching/cooling rate promotes the generation of uniform and ultrafine nanoparticles. Due to the uniform core−shell NiFe nanoparticles enhancing the electron transfer, the obtained catalysts by UTS showed a lower overpotential (179 mV at 10 mA cm^{-2}) than catalysts treated in the furnace. Similarly, it is found that the carbonized wood treated by CO_2-activation provided abundant carbon defects for anchoring quinary metal salts (Pt, Ni, Co, Fe, Cu) (Figure 9e).[99] The UTS offering a temperature of 2060 K ensured sufficient energy to drive the metal salt decomposing and recrystallization. The adjacent carbon atoms surrounded by metal nanoparticles could form a few-layer carbon shell by metal catalysis at high temperatures, thus forming an encapsulated high-entropy alloy. The stable interface between the high-entropy alloy and carbon shell not only reduced the overpotential but also improved the durability of hydrogen evolution. The CNT encapsulated Pt_1/WC_x nanostructures were prepared by the UTS; the UTS process promoted the in situ rapid conversion of Pt and W precursors that were encapsulated inside the carbon nanotube into Pt_1/WC_x nanostructures.[103] And the particle sizes were distributed at 2−5 nm due to the narrow nanotubes. Benefiting from the encapsulated structure and strong metal−support interaction of Pt_1/WC_x, it exhibited greatly boosted HER performance. More importantly, UTS can efficiently reduce the residual organics that may cover up the catalytically active sites on high-entropy alloys.[104] And the formation of N-doped carbon shells closely connected the high-entropy alloys with the carbon matrix, enabling superior HER performance.

3.2.2. Oxygen Evolution Reaction Catalysts. Currently, catalysts with rational electronic structures have been emerging as an attractive strategy for overcoming the kinetic barriers and enhancing the reaction kinetics of OER.[105] The introduction of heteroatoms with lower electronegativity, preparation of nanoparticles, and high-entropy materials are regarded as feasible strategies for modulating the electronic properties of catalysts. According to previous reports, the UTS technique is widely conducted to synthesize the above type of materials due to its unique merits.[92,106−109] Different metal salts, likely Fe, Mn, Ni, Zn, and Mg, mixed with Co salts through UTS treatment converted to M (Fe, Mn, Ni, Zn, Mg)-CoO, thus optimizing the local electronic structure of CoO, where Fe-CoO exhibited a low overpotential of 280 mV at 10 mA cm^{-2}.[110] Usually, the catalysts combined with the carbon matrix not only improve electron transfer but also expose the active sites. However, the interaction between the catalysts and the carbon matrix would affect the stability of the catalysts. UTS can render the metal nanoparticles loaded on the carbon matrix through stronger chemical bonds because of its in situ synthesis method. Due to the direct effect on the carbon fiber's surface by UTS, the electrochemical surface area (ECSA) may decrease; however, the incorporation of Fe could regulate the d-orbital electronic structure to improve the electrochemical performance.[111] Thus, the prepared RuFe@carbon fiber still manifested superior OER performance, which required 188 mV to achieve 10 mA cm^{-2} and maintain it for 600 h. Besides, the ultrahigh temperature can cause different evaporation of metals due to their different vapor pressures, thus achieving the unique structure of a thinner Fe shell layer (~2 nm) coated on $CoFeP_x$.[112] With the protection of in situ generation of the Fe shell layer, $CoFeP_x$ maintain the high catalysis activity.

The importance of high-entropy materials is not neglected in the OER because of their regulated defect structure and electron interaction among the various metal atoms, displaying grand promise for oxygen evolution as catalysts. Nevertheless, the thermodynamic immiscibility of the metal elements causing the effective preparation of high-entropy materials faces a challenge, especially since the room-temperature equilibria and Ostwald ripening suppress the possibility of conventional synthesis approaches for preparing high-entropy materials.[1] Conversely, the nonequilibrium process of UTS can easily drive the metal salt "fission" and "fusion" by rapid quenching and further form high-entropy materials. A temperature of up to 3000 K and heating rate of up to 10^5 K s^{-1} exceed the melting point of most metals, resulting in the creation of solid-solution nanoparticles with maximized configuration mixing entropy. Therefore, PtFeNiCoCu alloy nanoparticles uniformly distributed on the CNT were obtained by UTS.[113] The numerous defects, including vacancies, dislocations, and point defects that are beneficial to improving the OER activity, appear in the high-entropy alloys due to rapid heating. The lower electronegativity metals such as Ru, Mn, Cr, and V combined with other metals through UTS created the high-entropy oxides for OER,[114,115] and the electron interaction among the multimetallic elements also induced the generation of abundant active sites for boosting OER. For previous metal sulfides/phosphates limited to 2−3 metal elements, the mixtures consisting of metal salt precursors with a sulfur source or phosphorus source were treated with the UTS technique; the high-entropy metal sulfides $((CrMnFeCoNi)_x)$[116] and high-entropy metal phosphates $(CoFeNiMnMoPi)$[117] were synthesized for the first time and exhibited low overpotential and superior durability for the OER. Additionally, large amounts of RuMnFeMoCo nanoparticles compactly distributed on the carbon fiber were easily achieved by UTS that offered 1800 K in 1 s; this process addressed huge challenges caused by the immiscibility of metal elements and precisely controlled the size of particles (10−20 nm).[118] With the synergistic effects among the multiple metal elements, the catalytic activity and stability were further enhanced. While metal precursors were rapidly heated in air, the oxygen can be incorporated into the FeCoNiCuMo high-entropy framework, activating the lattice oxygen in OER.[119] The obtained FeCoNiCuMo-O performed with excellent OER activity by the optimization of the proton transfer in the lattice oxygen mechanism and intermediate *OH adsorption in the adsorption evolution mechanism.

3.2.3. Oxygen Reduction Reaction Catalysts. Engineering catalysts for oxygen reduction reactions plays a critical role in promoting the application of clean energy technologies. Extensive efforts have proven the metal-nitrogen-doped carbon catalysts boost ORR performance.[120−122] The size control, distribution, and content of pyridinic-N and pyrrolic-N of the catalysts are crucial for improving their ORR performance and stability. However, the conventional preparation of metal-nitrogen-doped carbon requires long-term high-temperature treatment, which leads to aggregation, large-size particles, and

https://doi.org/10.1021/acsnano.5c04768
ACS Nano XXXX, XXX, XXX−XXX

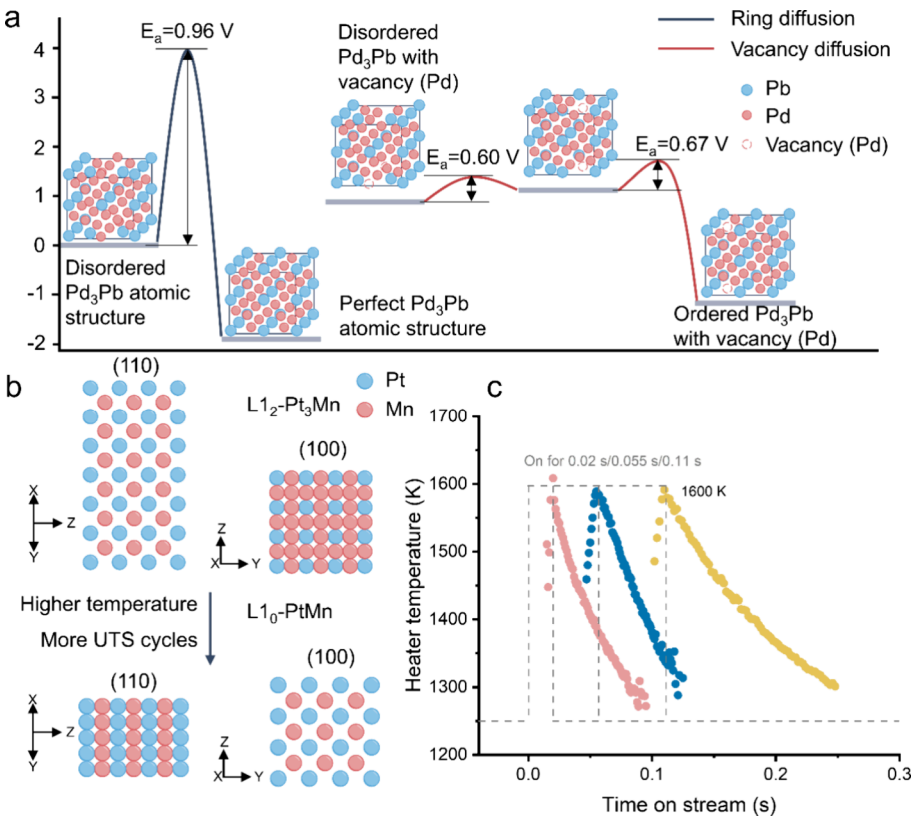

Figure 10. (a) Density functional theory calculation results for the formation of Pd_3Pb via the Pd vacancy diffusion and ring diffusion pathways. (b) The crystal structure of $L1_2$ Pt_3Mn and $L1_0$ PtMn. (c) Temporal profile of the carbon heater. (a) Adapted with permission.[127] Copyright 2022, American Chemical Society. (b) Adapted with permission.[128] Copyright 2024, Wiley. (c) Adapted with permission.[3] Copyright 2022, Springer Nature.

low content of N. Therefore, the reduction of ECSA, scarce amount of active sites, and inferior intrinsic activity of catalysts deteriorate their ORR electrocatalytic activity. The precise heating control and rapid ultrahigh temperature reaction properties of UTS offer an effective strategy to achieve the high-density, ultrasmall, and uniform metal-nitrogen-doped carbon ORR electrocatalysts and regulate the content of N.[123] It is found that the particle size of CoO/N/C can be tuned from 3 to 20 nm by adjusting the ratio between ZIF-67 and carbon powder under UTS reaction conditions.[121] The increased content of pyridine-N and graphitic-N derived from the ligand improved the specific surface area and enhanced the ORR activity. In another study, the content of pyridine-N and graphitic-N in Co nanoparticles loaded on porous carbon nanofibers (Co@N-C/PCNF) is higher than that of PCNF,[124] indicating the reduction of pyrrolic N and oxidized N and enhanced graphitization degree after the UTS process. Forming an ultrathin N-doped carbon layer coated on the surface of Co nanoparticles protected the Co nanoparticles from corrosion and inhibited agglomeration, thus ensuring superior ORR stability. However, it was found that the distribution state on carbon cloth of ZIF-8 would affect the resulting ZIF-8 derived catalyst properties through UTS treatment; more uniform distribution could bring superior properties.[125] Additionally, the rapid UTS process leading to vigorously diffused gases could result in a porous structure instead of dense and compact structures by a traditional furnace, and the porous structure could be further increased by increasing the heating rate. As a result, the Co−N−C samples synthesized by UTS exhibited a smaller particle size (1.9 nm) and larger ECSA (2350 cm^2) than that of traditional furnace pyrolysis, showing only a negative shift of 6 mV for the half-wave potential after 5000 cycles; importantly, the former synthesis method caused time reduction by at least ∼5 orders of magnitude.[126]

The ultrahigh temperature and rapid heating/cooling rate of UTS also make it possible to investigate the ORR intermetallic catalysts and ensure the effective synthesis of single-crystal structures. By rapid UTS to a temperature of 1600 K (heating rate of 10^5 K s^{-1}), the materials' structure underwent a disordered−ordered phase transition with the time increasing from 0.05 to 60 s, ultimately forming ultrasmall $L1_2$ Pd_3Pb intermetallic nanoparticles (∼6 nm) uniformly distributed on the carbon fibers.[127] In contrast, the materials obtained by conventional pyrolysis showed a larger particle size of ∼85 nm and a lower long-range order of 60%. The mass and specific activities of $L1_2$ Pd_3Pb by UTS are superior to those of conventional pyrolyzed Pd_3Pb. In addition, because of the lower vacancy diffusion activation energy barrier and greater vacancy generation during the rapid UTS process, the vacancy diffusion mechanism is considered the dominant pathway for forming $L1_2$ Pd_3Pb (Figure 10a). In terms of the formation of intermetallic structures, the metal precursor feeding ratio and UTS parameters, including shock cycles and temperature, also caused the generation of different structures. It was found that increasing the shock cycles drove the gradual diffusion of Mn atoms into the Pt lattice, and well-defined $L1_2$ Pt_3Mn could be obtained after 12 cycles of UTS.[128] Notably, on adjustment of the Pt:Mn feeding atomic ratio to 1:1, the atomic arrangement showed the ordered $L1_0$ PtMn structure. When the number of

https://doi.org/10.1021/acsnano.5c04768
ACS Nano XXXX, XXX, XXX−XXX

UTS cycles increased to 13 or the heating temperature increased, $L1_0$ PtMn gradually converted into $L1_2$ Pt_3Mn due to its lower formation energy (−0.354 eV $atom^{-1}$) (Figure 10b). Due to the higher work function of $L1_2$ Pt_3Mn, it displayed an excellent half-wave potential (0.91 V).

3.2.4. CO_2/Nitrogen Reduction Reaction Catalysts. The increment of greenhouse gases like CO_2 causes global warming and seawater acidification. Therefore, the efficient conversion of CO_2 to valuable chemicals has attracted tremendous attention and is considered a feasible approach that not only reduces its negative impact but also produces economic and energy profits.[129] Electrocatalysis reduction of CO_2 shows promising potential to convert CO_2 into formate and C1 products. However, the preparation of high-performance electrocatalysts remains a grand challenge.[130] In terms of single-atom catalysts, metal centers are coordinated with nonmetal dopants to form a stable structure, such as Fe-N_x,[131] Co-N_x,[132] and Ni-N_x,[133] and the obtained coordination chemicals play a critical role in electrocatalysis. An excess content of N dopants will damage the CO_2 catalysis performance and selectivity due to the form of pyrrole N, pyridine N, graphitic N, and N-O. Improving the coordinated N dopants and reducing the uncoordinated N dopants should be an effective strategy for achieving the desired metal-N_x structure. The UTS technique was adopted to successfully synthesize carbon-supported Ni-N_x, which includes 80% N dopants coordinated with Ni centers.[134] It also suggested that UTS drove Ni and N coordination and reduced uncoordinated N dopants. As a result, the as-prepared carbon-supported Ni-N_x exhibited enhanced CO_2RR catalytic activity and stability. Besides, the carbon fibers can be modified with polytetrafluoroethylene (PTFE) by UTS, and the functional carbon fibers are favorable for constructing a Mott−Schottky heterointerface and promoting the in situ transformation of Bi_2S_3 solid nanorods into interconnected 3D Bi nanosheets, exposing more edge active sites and accelerating the electron transfer toward to improve CO_2RR performance.[135] In addition, the rapid UTS had no significant effect on the morphology of the Bi MOF nanosheets compared to the ball milling treatment.[136] And the high temperature weakened Bi−O coordination strength and promoted the generation of more Bi vacancies on post Bi^0 catalysts. The significant tensile strain on adjacent nondefective Bi sites posed by more Bi vacancies enhanced the adsorption of the *OCHO intermediate and activated more distant Bi sites, thus giving a remarkably high Faradaic efficiency for the formate production of catalysts. Due to the important role of heterojunction in the catalysis, the ultrahigh temperature of UTS offered more stabilized oxygen species in In_2O_3 during the subsequent electrochemical reduction,[137] thus suppressing the excess reduction of In_2O_3 to form an In/In_2O_3 heterojunction. The higher temperature UTS treatment can increase the number of more stable oxygen species in the In_2O_3. During the electrocatalysis CO_2 test, the obtained catalysts displayed a Faradaic efficiency of close to 100% for C1 chemicals. And the incorporation of oxygen into the copper clusters by UTS could result in asymmetrical atomic and electronic structures. The formation of Cu_4O-Cu/C_2O_1 and Cu-N_1O_1 moieties could regulate the adsorption energy of intermediates to promote the conversion of CO_2.[138,139]

Besides, the UTS technique is applied to fabricate NRR catalysts. Although UTS has been demonstrated to provide sufficient energy to promote the generation and uniform distribution of nanoparticle catalysts, the selectivity, rate, and yield of high-value-added chemicals at low energy costs should be further improved. Based on the UTS technique, the programmable heating and quenching method that operates with rapid switching between low and high temperatures in just milliseconds was proposed (Figure 10c).[3] Compared to UTS with continuous steady-state conditions, this method provides a new sight to tune by a controllable temporal temperature pattern and, combined with previously reported data,[140] science approaches can reduce the experimental effort, thus improving the efficiency. Utilizing this method, Ru nanoparticles loaded on carbon felt as catalysts exhibited high NH_3 production and superior stability. Of course, UTS with heating at constant temperature still features many advantages compared to traditional furnaces. MIL-125 (Ti) with ferric nitrate after UTS (300 A, 20 s) converted into smaller Fe-doped anatase TiO_2 with more oxygen vacancies,[141] where the content of oxygen vacancies was higher than that of Fe/TiO_2 treated by a traditional furnace. The Fe/TiO_2 obtained by UTS also exhibited an ammonia production rate of 56.87 μmol g^{-1} h^{-1}. Similarly, two UTS treatments not only generated oxygen vacancies but also induced the formation of Ru nanoparticles.[142] Benefiting from the vacancies and Ru nanoparticles, the final samples showed an improving ammonia evolution performance.

4. RECYCLING SPENT BATTERIES THROUGH ULTRAFAST THERMAL ENGINEERING

The widespread adoption of LIBs not only causes the explosive demand for critical minerals (lithium, cobalt, and nickel) but also confronts the formidable challenge of disposing of spent LIBs, achieving the end of their lives.[143] Especially, improper disposal will indispensably lead to deleterious effects on the environment and the waste of mineral resources. Recently, direct recycling techniques by UTS are proposed and exhibit enormous advantages as alternatives to conventional recycling methods, including pyro- and hydrometallurgical, which are intrinsically destructive to the electrode materials. The ultrahigh temperature and short reaction time properties of UTS can provide a kinetics-dominated and thermodynamically nonequilibrium environment for rejuvenating degraded electrode materials,[144] thus improving recycling efficiency.

4.1. Recycling of Cathode Materials. The commercial LIB cathodes are composed of lithium, cobalt, nickel, manganese, and so forth, which are predominantly collected from natural resources in the long term. However, the limited reserves of battery metals, especially cobalt and nickel, face a formidable depletion issue. Thus, efficient recycling of spent cathodes of secondary LIBs is essential to mitigate the scarce supply of battery metal resources; namely, spent cathodes serve as metal mineral resources for producing battery metals. Pyrometallurgy[145−147] and hydrometallurgy[148−150] are typical commercial recycling strategies to recover valuable metals in spent LIBs. The pyrometallurgy process requires substantial energy consumption for high-temperature furnaces, and hydrometallurgy methods usually cause a large amount of secondary wastewater because of a strong reliance on a high-concentration acid to afford high yields. Apparently, these two methods are energy-intensive and time-consuming and have an environmental footprint. As a result, a rapid, effective, and eco-friendly recycling approach is urgently desired to develop for regenerating cathodes and industrial application.

https://doi.org/10.1021/acsnano.5c04768
ACS Nano XXXX, XXX, XXX−XXX

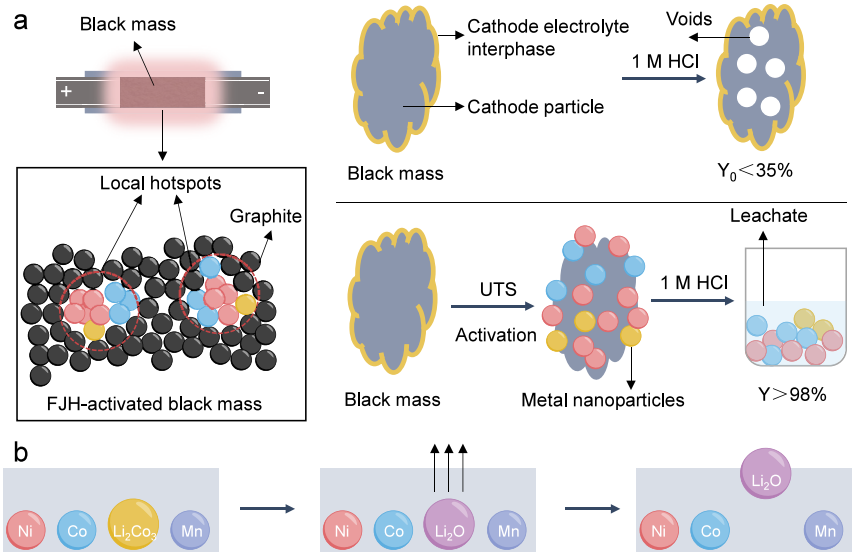

Figure 11. (a) Illustration of the UTS activation of black mass, the local hotspots of resistive cathode particles, and the acid leaching results with and without UTS activation. (b) Schematic illustration of the formation of Li_2O during the UTS process. (a) Adapted with permission.[154] Copyright 2023, American Association for the Advancement of Science. (b) Adapted with permission.[155] Copyright 2023, Wiley.

For collecting valuable metals, it is inevitable to use acid or water to leach metals, which is determined by their chemical characterization. Thus, research about reducing the amount of acid or water has attracted increasing attention in the recycling area because of the complex composition of cathodes, including Li, the high valence of Ni, Mn, Co, organic binder, and conductive carbon, which cause low leaching efficiency. To achieve the above targets, researchers have adopted the UTS method to recover the cathodes.[151,152] Before the leaching process, the valence of Ni, Mn, and Co can be reduced under the carbothermal reduction during the UTS process, which is conducive for subsequent leaching.[153] The carbonized organic binder and conductive carbon also can guarantee the current passing for in situ generation of Joule heating and serve as a reductive agent to accelerate the reduction of metals. Notably, accurate control of temperature and reaction time is essential to obtain high yield and utilization of dilute acid. Additionally, the cathode particles and SEI layer show a higher resistance than conductive carbon and graphite, requiring a larger power to trigger the thermal transformation to activate the black mass by local Joule heating (Figure 11a). Therefore, Tour's group reported that the suitable applied flash voltage and duration time are 80 V (~2100 K, peak current at ~104 A) and 110 ms,[154] which activate the black mass and improve the recovery yields for battery metals to 286%, compared to the direct leaching by 1.0 M HCl. When increasing the voltage and reaction time, the higher temperature would cause the evaporation of metals, such as lithium, thus leading to the loss of metals. Moreover, the UTS-activated black mass without pretreatment for removing SEI and electrolyte can maintain stability under ambient conditions without an inert atmosphere, reducing the operation cost and environmental pollution. The trace metal contributions from the UTS equipment like quartz tube, copper, and graphite spacers are also validated and ignored in the calculations. In order to efficiently separate the valuable metals in the recycling process, different leaching solutions can be applied to different metals. For example, the collection of Li can be achieved through water leaching. However, the phase of Li after high-temperature treatment is essential to recycle Li, where Li would usually be transformed into low-solubility Li_2CO_3, thus lessening the recovering efficiency. According to reports, Li_2CO_3 can be decomposed into Li_2O at higher temperatures, which is a higher solubility phase. Thus, the UTS process with an ultrahigh temperature can facilitate the decomposition of Li_2CO_3 into Li_2O. With the increase of current from 100 to 200 A, the higher solubility of Li_2O starts to form with the reaction time exceeding 30 s at 180 A or 20 s at 200 A, leading to a higher concentration of Li in the leaching solution than traditional high-temperature reduction process.[155] As shown in Figure 11b, during the UTS process, the Li_2O first evaporated from the inside of the cathodes because of its higher vapor pressure than others and recrystallized on the surface, forming small particles due to the rapid cooling rate and short reaction time. Meanwhile, the lower valence of Co, Ni, and MnO that are composed of predominant phases are beneficial to subsequent leaching treatment.[154]

The nondestructive regeneration of cathodes and their continued application in the second battery are other paramount research directions in the recycling area. For the regeneration of spent cathodes, various methods, including molten salt,[156] solid-state sintering,[157] and hydrothermal,[158] have been developed. However, the high-energy consumption, long-term and incompletely recovered phase structure, and electrochemical performance are not ignored. For example, the long-term high-temperature treatment of cathodes will cause the partial loss of lithium source and possibly a corrosive reaction between $LiCoO_2$ (LCO) and the container, thus affecting the regeneration efficiency. Therefore, the instantaneous reaction under an ultrafast heating rate is necessary to regenerate the LCO, whereas the UTS method allows a much higher temperature, heating rate, and faster reaction rate within seconds to repair the phase structure and performance of LCO. In the long-term cycles of LCO, the spinel Co_3O_4 formed on the surface of LCO would exacerbate the layered structure and electrochemical performance. During the UTS process,

https://doi.org/10.1021/acsnano.5c04768
ACS Nano XXXX, XXX, XXX−XXX

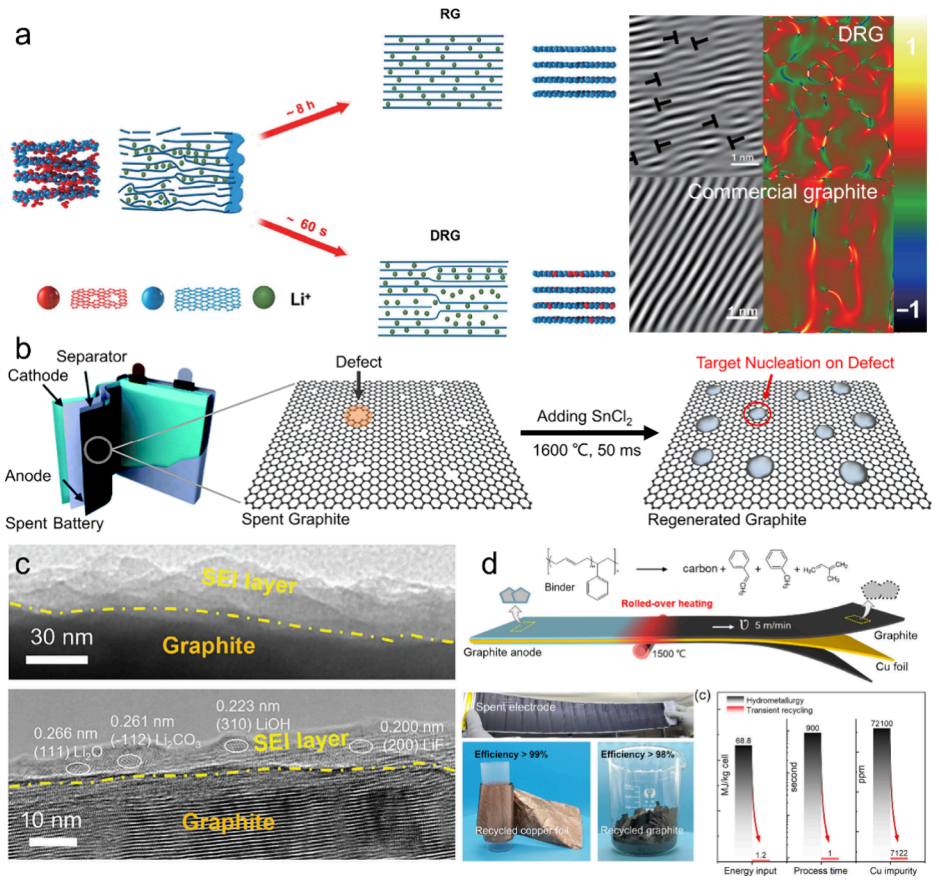

Figure 12. (a) Schematic diagram of recycling of anodes and HRTEM images. (b) Upcycling process of spent graphite by UTS. (c) The TEM images of SEI after UTS treatment. (d) Schematic illustration of recycling of spent graphite by rolled-over heating and comparison of energy input and process time of different recycling processes. (a) Reproduced with permission.[173] Copyright 2022, Springer. (b) Reproduced with permission.[176] Copyright 2023, Wiley. (c) Reproduced with permission.[189] Copyright 2023, Wiley. (d) Reproduced with permission.[190] Copyright 2023, Royal Society of Chemistry.

increasing the temperature above 1440 K can remove the Co_3O_4 due to its unstable property at high temperature; however, this process also lessens the content of Co in the regenerated cathodes.[159] Thus, it is necessary to convert Co_3O_4 to LCO for the utilization of Co components. With the introduction of extra lithium sources like $LiCO_3$ into the spent LCO under 1440 K for 8 s, the lithium vacancy and spinel Co_3O_4 can be completely repaired, and the phase structure and electrochemical performance are both restored. Additionally, the high temperature field generated from UTS can be transiently exerted through each bulk $LiFePO_4$ crystal, thus triggering the swift and coherent Li−Fe interatomic reordering from the unit cell to unit cell in milliseconds and bypassing the onset of potential detrimental side reactions.[160] While polyvinylidene difluoride binder can be carbonized with F-doped carbon in mere milliseconds, the repaired $LiFePO_4$ particles further were coated by the binder-derived carbon to achieve a high initial Coulombic efficiency, rate performance, and stability. Because of the complex composition of spent cathodes, the number of impurities, such as Al^{3+} and Cu^{2+}, in the regeneration of cathodes can deteriorate the electrochemical performance, where Al and Cu from the current collector can result in specific capacity decay and polarization buildup, especially in the traditional regeneration process. The UTS method can provide sufficiently high temperature (~2500 K) in milliseconds to reduce the amount of Al and Cu contamination because of their higher vapor pressure, which meets the requirement of the safety content threshold of impurities (~100 ppm).[6] In addition, extra conductive carbon like carbon black, graphite, and mixing cathodes before the UTS process is indispensable; it can improve the electrical conductivity of the mixture, guaranteeing that the current can mainly pass through the carbon to provide the local carbothermal reduction environment for cathodes.

4.2. Recycling of Anode Materials. In contrast to cathode material recycling, the recycling of graphite anodes in spent batteries has been mostly neglected due to abundant reserves of natural graphite and the relatively low economic value of recycling graphite. For the large quantity of graphite in spent batteries, direct incineration for energy or landfilling have become the general treatment, which not only increases greenhouse gas (GHG) emissions but also causes the waste of carbon resources. As an important strategic resource, the effective recycling of graphite in spent batteries can reduce the environmental pollution caused by spent batteries and create a balance between the supply and demand of the carbon market. Currently, the predominant commercial recycling methods are divided into two types, namely pyrometallurgy and hydrometallurgy methods.[146,149] These methods both mainly focus on the recycling of high-value metals (such as Co, Ni, and Cu) in graphite; the pyrometallurgy method obtains the recycling metal by high-temperature carbothermal reduction while the graphite is directly burned, causing the serious waste of graphite and CO_2 emission.[161] Although hydrometallurgy can

https://doi.org/10.1021/acsnano.5c04768
ACS Nano XXXX, XXX, XXX−XXX

effectively collect metal and graphite, this process is generally accompanied by a large amount of wastewater, increasing pollution and hazards.[162,163] Additionally, pyro- and hydrometallurgy methods both face the difficult removal of inert binder and perishable SEI from the spent graphite. Therefore, more rational and environmentally friendly recycling methods should be developed to cope with the enormous recycling market for graphite and improve the recycling efficiency of graphite. Recently, direct recycling of graphite has been proposed and has received a lot of attention from researchers; this method can directly recover the anode materials and protect the original structure from destroying or repairing the defect of graphite caused during the cycling process, thus harvesting the active materials or high-value functional materials with less pollution, energy, and time consumption.[164−166]

The high-temperature treatment is considered the most suitable for recycling the spent graphite, which can effectively remove the inert binder and SEI, repair the defects caused during the long-duration cycles, and decrease the resistive impurities.[167,168] However, the ultrahigh temperature graphitization (about 3000 K, even lasting for several days) of anode graphite by traditional calcination methods has a high requirement for energy and time cost, accounting for more than 50% of the recycling cost.[169] The UTS method, with the advantage of energy and time, is employed to recycle the spent graphite and is considered a promising recycling method by ultrahigh temperature treatment in the recycling of spent electrode materials. Especially in the removal of SEI and binder from the spent graphite, the UTS method is absolutely superior compared to other methods. During the calcination process, the temperature can easily achieve more than 3000 K in a short time of 0.01 s, and this temperature has exceeded the thermal-decomposed temperature of the binder (<600 K), the component of SEI (volatilization temperature of LiF <1500 K, boiling temperature of $LiCO_3$ <1700 K), and inserted lithium (<1600 K) in the graphite layer.[167] There is no observation of the SEI layer in the recycled graphite after UTS treatment, and the binder is converted to small particles attached to the graphite sheet through carbonization. Under the effect of ultrahigh-temperature shock, the defect of spent graphite can be repaired, and the degree of graphitization is also enhanced. The recycled graphite restores the original structure of graphite and shows a similar electrochemical performance to commercial graphite, which demonstrates that the UTS strategy can be applied to upcycle the spent graphite anode to recover the original properties of graphite. However, a large number of defects in cycled graphite anodes is a mixed blessing; it can cause inferior graphitization and usually damage the electrochemical performance.[170] Meanwhile, the defect sites in the layered graphite can lower the Li^+ insertion and extraction energy barrier to improve the diffusion kinetics of Li^+.[171,172] Therefore, restoring the partial defect of the spent graphite during the UTS process would be beneficial to improve the electrochemical performance of recycled graphite, which preserves the original partial dislocation and can form a large number of dislocation dipoles with opposite Burger vectors inducing dense compressive-tensile strain fields due to the high temperature and short calcination process (1500 °C, 60 s) of the UTS strategy (Figure 12a), thus lowering the total strain energy and improving the transition kinetics from LiC_{12} to LiC_6.[173−175] Nevertheless, within the high-temperature and long-term calcination process of the traditional annealing treatment, the dislocations gradually move to the edge of the crystal and eventually disappear. Therefore, the recycled graphite with partial defects exhibits a satisfactory rate performance of 323 mAh g^{-1} at 2 C, which is higher than that of commercial graphite (120 mAh g^{-1}). Although increasing the calcination temperature and time with the UTS process both repair the defect in the spent graphite generated during the charge/discharge process, enhancing the electrochemical properties of recycled graphite, it sacrifices the energy and time (>3000 K or ∼60 s). A recent study reported that the introduction of a lower content of nanoscale metal healant with a low melting point also remediates the defects like vacancies in the spent graphite through the UTS process to enable the full utilization of the advantages of shorter time consumption.[176] Under high temperatures, $SnCl_2$ is rapidly reduced to Sn, which further converts into a molten and dynamic state to repair the defects due to the much stronger binding energy between Sn and defects in spent graphite (Figure 12b), and this process only requires a temperature of 1600 °C and 50 ms. It is notable that the vapor pressure also rapidly increases from 12.7 to 745 Pa with the temperature increasing from 1400 to 1800 °C, which would lead to obtaining fewer Sn nanoparticles dispersed on the surface of spent graphite. To achieve superior electrochemical performance, the optimal temperature of 1600 °C enables an appropriate balance between defect repairing and Sn nanoparticle size. Therefore, it is important to control an accurate reaction temperature that may influence the thermal-dynamical process and regulate the microstructure of desired products.

Taking cost and electrochemical performance into consideration, most recycling research overlooks the collection of the transition metals in the graphite owing to their high boiling points (∼3200 K for Co, Ni), requiring extensive energy and destroying the structure of graphite. To reduce energy consumption and improve efficiency, the recycling of high-quality graphite requires a relatively low temperature and a short reaction time. In order to eliminate the metals for further recycling, concentrated acids are the main selection, but this process usually causes intensive waste streams and suffers from low efficiency.[177−179] The main reason for the difficult removal of transition metals is that they exist in the high-valence-state compounds, which exhibit a larger Gibbs free energy of the acid dissolution reactions for the metals compared to the lower valence state.[153] According to prior research, the utilization of an extra reagent to lower the valence state of metal facilitates the dissolution reactions for the metals,[180,181] and leaching transition metals in the spent graphite only requires the dilute acid after the reduction reaction of the metal, reducing the generation of water waste. UTS methods can lower the valence state of the metal through electrothermal reduction. Therefore, the recycling efficiency of transition metals can be improved by collecting metals from recycled graphite by using dilute acid (e.g., 0.1 M HCl).[153] Meanwhile, the bulk structure and graphitization of recycled graphite cannot be destroyed, guaranteeing the electrochemical performance of recycled graphite. The cooperation between the UTS process and dilute acid treatment can obtain both the recycled graphite and high-value metal, providing a profitable strategy for recycling the spent graphite anodes.

On the other hand, the UTS method provides ultrahigh temperatures to destroy the perishable SEI formed on the surface of graphite.[153,167,173,176] However, the higher Coulombic efficiency determined by the SEI is the most important

https://doi.org/10.1021/acsnano.5c04768
ACS Nano XXXX, XXX, XXX−XXX

index for lithium batteries, which represents the consumption of active lithium. There are extensive reports that have paid more attention to improving the Coulombic efficiency through reducing or compensating the irreversible lithium loss, such as prelithiation,[182−184] development of novel electrolytes,[185] and artificial SEI;[186−188] the implementation of these strategies relies heavily on the external lithium sources. The formed SEI on the surface of the spent graphite and residual lithium in the spent graphite layer provide a promising strategy to improve the Coulombic efficiency and compensate for the lithium rather than the above approaches. However, the UTS temperature approaches employed in the rejuvenation of spent graphite almost remove the SEI and residual active lithium, leading to obtaining carbon-attached recycled graphite without reusing the valuable SEI and active lithium. Rationally controlling the process of UTS (1900 K for ∼150 ms) can achieve the reservation of inorganic components in the original SEI and residual active lithium,[189] thus reducing the need for external lithium sources to construct the SEI or compensate lithium. The formation of a compact inorganic (Li_2O, Li_2CO_3, LiOH, and LiF) layer covered on the surface of recycled graphite after the rapid UTS process not only eliminates the demand of prelithiation but also enhances the toughness and durability of the SEI for better cycle stability (Figure 12c). The obtained recycled graphite exhibited an initial Coulombic efficiency (104.7%) higher than that of commercial graphite (87.3%). Additionally, the direct UTS approach simplifies the upcycling process of degraded graphite, significantly improving the manufacturing cost, energy consumption, and pollution emission compared to traditional pyro- and hydrometallurgy methods with cumbersome processes. The recycling strategy of the graphite anode accompanied by reusing the SEI and residual active lithium also offers an innovative route for the upcycling of the spent graphite to drive the closed-loop sustainability of batteries.

The direct recycling method by UTS certainly rejuvenates the superior graphite anodes with much less energy, time, and waste, but this ideal strategy and traditional pyro- and hydrometallurgy strategies both meet a formidable challenge. The prior step in the recycling process is the separation of anode materials from the current collectors, which is a difficult process due to the vigorous binder and ample compacted dense electrode. In most reports about direct recycling, the anode waste powders were collected from the current collector through shredding electrodes,[190] furnace calcination,[191] electrochemical separations,[192] and acid scrubbing strategies.[193] However, fewer impurities usually reside in the anode powders (e.g., ∼7 wt % Cu in graphite). Moreover, most recycling is adapted to address the recycling of spent batteries. For another recycling area, spent electrodes generated in the manufacturing of batteries are overlooked. In a recent study, the recycling of spent electrodes was considered as a research focus, which presents the relation among the peeling off, temperature, and time during the UTS process (Figure 12d).[190] The successful stripping of graphite from the copper collector is attributed to the fast heating rate and the heating uniformity of UTS throughout an electrode thickness of 132 μm, which enable the complete decomposition of binder and separate graphite. In this report, the optimal temperature and time are 1500 °C and 1000 ms, but the graphite could be peeled off from the collector as long as the calcination time exceeds 50 ms. The obtained graphite and copper current collector displays a high collection ratio of 98.7% and ∼100% intact copper foil. Meanwhile, the obtained graphite shows an excellent LIB performance with 340 mAh g^{-1} at 0.5 C.

5. EFFORTS TOWARD EQUIPMENT FOR SCALE-UP

The exceptional advantages of UTS make it an attractive method for the rapid synthesis/recycling of energy materials in laboratory research, but it remains a great challenge to fabricate materials continuously for scale-up. For the laboratory application of UTS, two classic type reactors, including quartz tubes[12] and carbon fibers,[194] were widely used to achieve the UTS process. The small devices based on these two reactors have been designed at the laboratory scale at present and show tremendous possibilities for scale-up in industrial production. One type of small device is shown in Figure 13a; the integrated

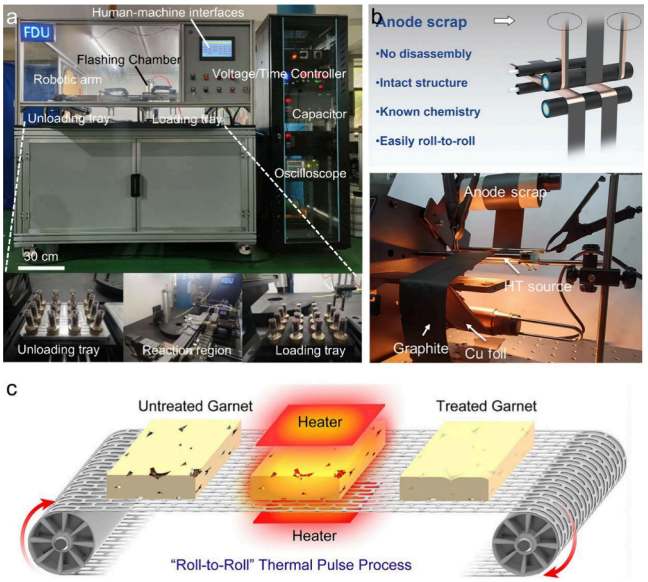

Figure 13. (a) Pilot-scale fabrication device of flash graphene. (b) Diagram and photograph of the anode scrap and roll-to-roll recycling of anode scrap. (c) Roll-to-roll device for UTS treatment of ceramic materials. (a) Reproduced with permission.[195] Copyright 2024, Springer Nature. (b) Reproduced with permission.[190] Copyright 2023, Royal Society of Chemistry. (c) Reproduced with permission.[79] Copyright 2019, Elsevier.

device controlled by a programmable logic controller gave continuous biomass flash graphene.[195] This equipment is made up of many independent quartz tube reactors, and the reaction process is similar to that of the laboratory device. Therefore, this enables the production of higher-quality products. Moreover, based on UTS's rapid heating rate and shorter reaction time, roll-to-roll equipment was self-made to recycle spent batteries (Figure 13b).[190] The anode scrap tape passed through the graphite heater and mechanical stress part at a speed of 5 m min^{-1}, followed by the rejuvenated exfoliated graphite, and fell into a collector continuously. Meanwhile, the Cu foil with a clean surface was collected on the roller. It is more suitable for the battery industry to recycle electrode scraps. In addition, other roll-to-roll equipment was created to process powder or pressed bulk (Figure 13c);[79,154,196] the current through the two graphite electrodes was directly conducted through the powder or pressed bulk. This device is suitable for the continuous, large-scale, and high-temperature treatment of materials, and the product efficiency can be improved by adjusting the movement rate of the conveyor belt.

https://doi.org/10.1021/acsnano.5c04768
ACS Nano XXXX, XXX, XXX−XXX

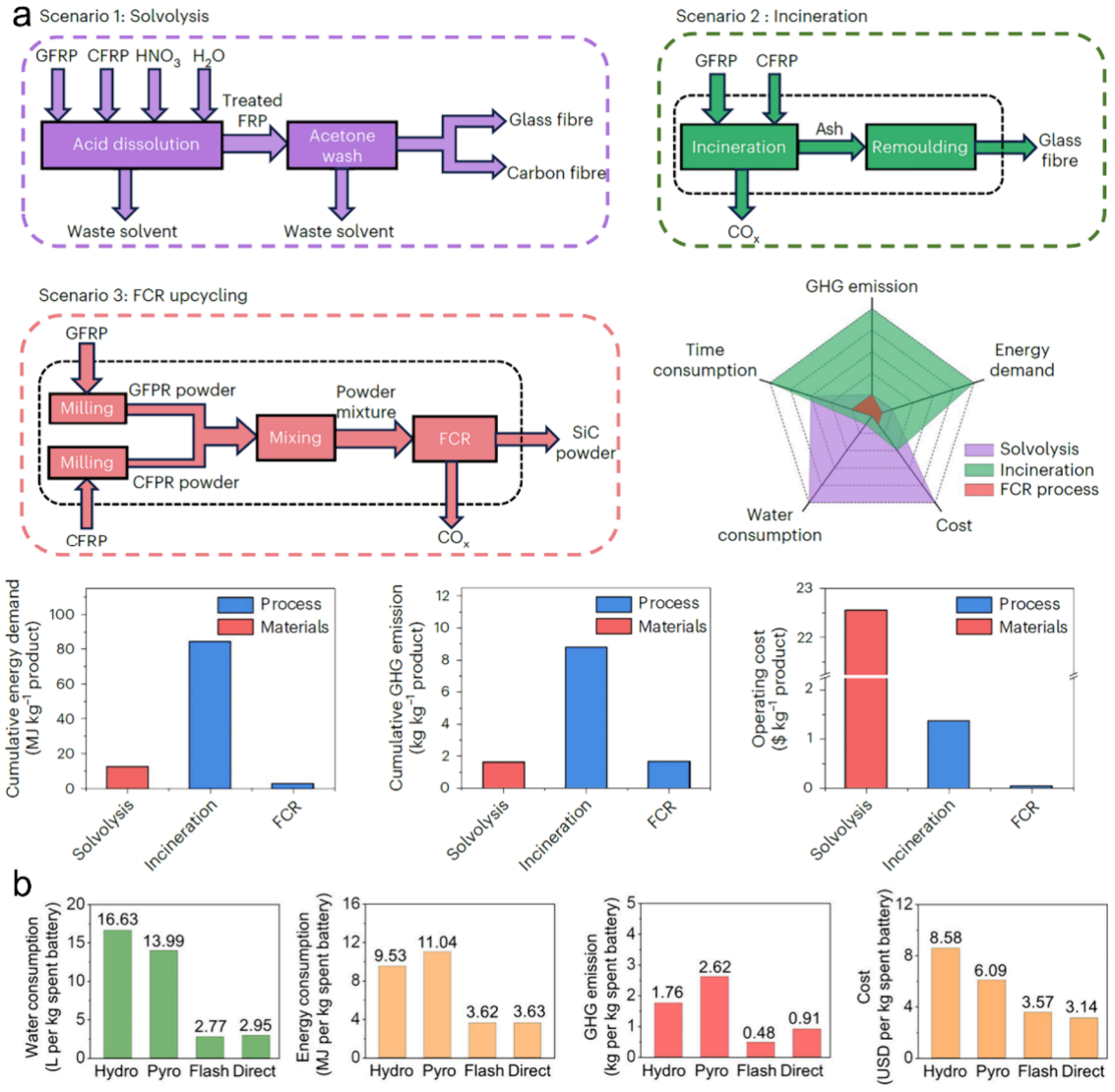

Figure 14. (a) Life cycle assessment for fiber-reinforced plastic recycling. (b) Water consumption, energy consumption, greenhouse gas emission, and cost analysis of different regeneration processes. (a) Reproduced with permission.[52] Copyright 2024, Springer Nature. (b) Reproduced with permission.[6] Copyright 2024, Springer Nature.

These efforts indicate a feasible, effective, and convenient strategy for rendering large-scale manufacturing by UTS, providing intensive potential for scale-up preparation of energy-related materials. However, the ultrahigh temperature during the reaction process puts forward higher requirements for the roll-to-roll reactor design. For example, a heater must have a high melting point, stable mechanical structures, and stable chemical properties, which can resist melting or evaporation, abrasion or distortion, and oxidation or reduction, respectively.[144] Besides, a uniform heating zone should be considered for the scale-up equipment, ensuring the reaction uniformity to obtain pure products. The high voltage and high temperature may cause a safety risk, and reasonable protection in the reactor design should be fully considered to protect the operators from danger. Besides, the high cost of electricity and substantial investment required for equipment have also been confronted in the industrial production system, including equipment replacement and electric system modification.[197] Thus, scaled-up UTS should solve these considerable challenges to realize the development of this technique.

Although devices on UTS have been developed to adopt scale-up, they still suffer from a formidable challenge that arose from the high-quantity heater and substantial cost of electricity.[144,197] First, the heater, as the most critical part of the equipment, must entail a high melting point and stable mechanical and chemical properties to bear melting or evaporation, abrasion or distortion, and reduction or oxidation, respectively. Second, there is a substantial capital investment for electric systems and UTS reactor devices before the traditional chemical synthesis reactor can be replaced by the electrothermal reactor. Despite electricity being more economically valuable than heat, the high cost of electricity remains a challenge to be confronted. Finally, the predominant advantages of UTS devices over conventional chemical reactors should be exploited at meaningful scales, which will help to promote their large-scale industrial application.

6. ENVIRONMENTAL AND ECONOMIC ANALYSIS ASSESSMENT

The environmental and economic analysis or benefits of the UTS technique are considered important indicators for

https://doi.org/10.1021/acsnano.5c04768
ACS Nano XXXX, XXX, XXX−XXX

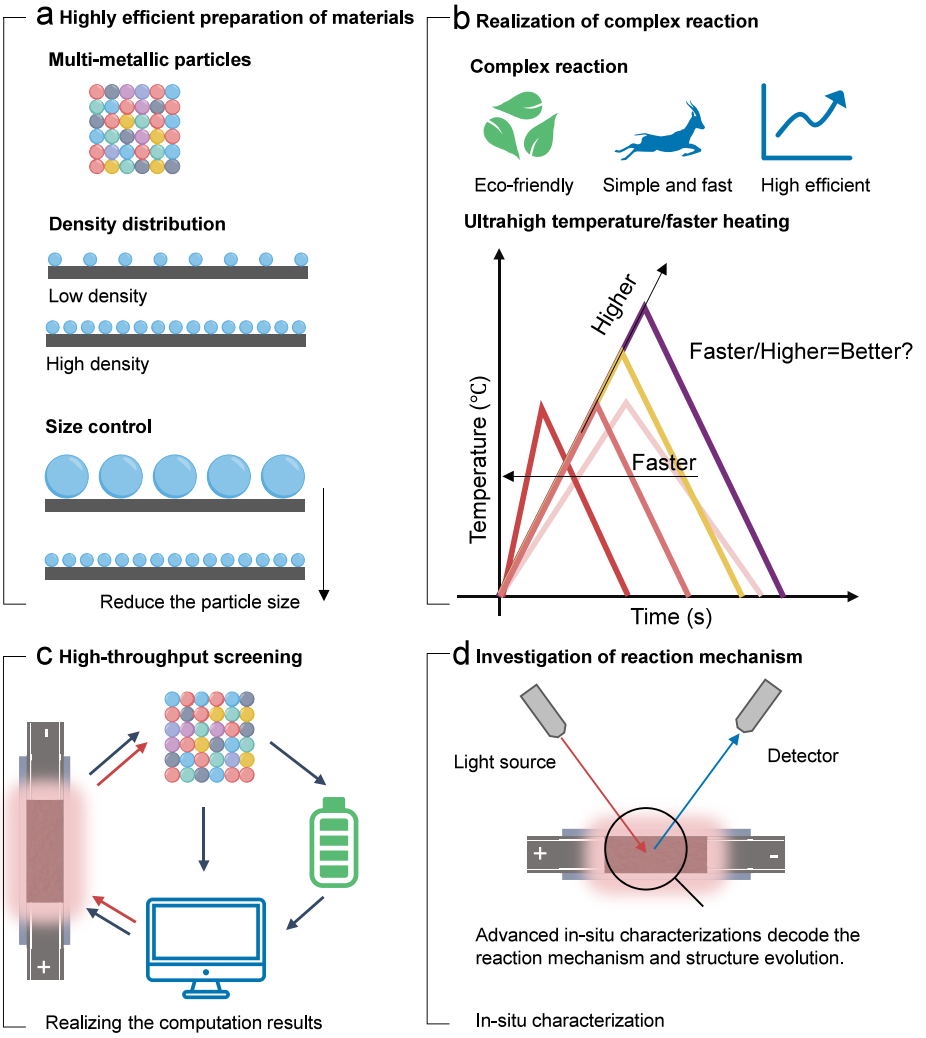

Figure 15. Perspective and current challenges of UTS in the (a) highly efficient preparation of materials, (b) realization of complex reactions, (c) high-throughput screening of materials, and (d) investigation of the reaction mechanism.

assessing its business value.[153,198] On the one hand, environmental protection must be confronted in industrial production. On the other hand, the production cost and profits are also related to the environment. Compared to traditional synthesis or recycling methods, the advantages of UTS are not only reflected in time and energy efficiency but also reduce pollution and improve economic profits.[154] GREET 2020[199] and Everbatt 2020[200] software developed by Argonne National Laboratory, are usually utilized to analyze environmental and economic profits. For instance, the UTS process only requires an energy demand of 2879 MJ tonne^{-1}, which is significantly lower than those of solvolysis and incineration methods for recycling fiber-reinforced plastics.[52] Regarding GHG emission, the emission of UTS is 1709 kg tonne^{-1}, which is close to that of solvolysis (1669 kg tonne^{-1}) and lower than that of incineration. The costs of 1 kg of SiC for UTS, solvolysis, and incineration are US$0.047, US$22.577, and US$1.386, respectively (Figure 14a). In the recycling of electrodes, the UTS method can decrease the consumption of water and energy over the hydrometallurgical and pyrometallurgical methods.[6] Besides, the GHG emissions and the cost can be further reduced by ~72% and ~58% (Figure 14b). These values suggest that the UTS technique has great environmental and economic benefits compared with other conventional methods.

7. EXTENSIONS AND OUTLOOK OF ULTRAFAST THERMAL ENGINEERING

The rapid development of energy storage and conversion devices is put forward to quickly exploit higher efficiency energy-related materials, including electrodes, current collectors, and catalyst production, thus satisfying the ever-increasing demands. Meanwhile, extensive numbers of energy devices, due to their poor performance or retirement period, need to be recycled for sustainability and environmental protection. These issues underscore the urgent requirement for a feasible, time-saving, and eco-friendly approach to developing or recycling energy-related materials. Ultrafast thermal engineering, especially ultrahigh temperature shock technology possessing a rapid heating/cooling rate, high temperature, and fast reaction process, enables a highly efficient, time- and energy-saving, nonequilibrium, fast kinetic rate, environmental, and profitable strategy for addressing these issues and has attracted more and more attention. Consequently, its work mechanism development and application in the synthesis and recycling of energy materials are discussed in detail for a deeper understanding of this approach, and it also offers more possibilities for

https://doi.org/10.1021/acsnano.5c04768
ACS Nano XXXX, XXX, XXX−XXX

researchers in exploring or recycling materials and developing advanced experimental and scale-up devices.

Despite a series of very successful works utilizing the UTS technology that have been achieved for energy-related applications, there is still tremendous potential to be developed for preferably applying this method in the future. To further promote the development of UTS, the referable and valuable contents as follows can be considered before relevant research.

(1) UTS technology provides more possibilities for synthesizing energy storage and conversion materials (Figure 15a). However, UTS confronts the challenge of precise control of the preparation of multimetallic particles, different density distributions, and size control. More control parameters should be considered to further ensure the controllability of the UTS process.

(2) The selection of UTS and conventional methods can be determined by the types of ideal samples, reaction temperature, environment, and cost (Figure 15b). UTS can provide more opportunities to realize the complex preparation process that needs high temperature (>1200 °C) and high enthalpy. The traditional furnace method is proper for preparing materials with special morphology structures like hollow, core−shell, and multishell. However, the reaction condition of UTS should be determined by the properties of materials; a faster heating rate or higher temperature is not necessarily favorable for preparing any materials. Thus, more efforts should be devoted to the controllable synthesis of nanomaterials with specific morphology.

(3) The realization of machine learning and theoretical computational predictions can be achieved successfully by UTS (Figure 15c). Its rapid reaction process ensures high-throughput synthesis and screening for various novel high-performance materials, accelerating the development of perfect materials. Importantly, the combination of UTS and artificial intelligence should be introduced to find the effective reaction parameters to solve the control of morphology and structure of materials.

(4) The reaction mechanism of the UTS process should be investigated deeply by novel characterization, thus guiding its wide application (Figure 15d). Although the structure alternation of materials after UTS treatment is attributed to the rapid reaction kinetics provided by the rapid heating/cooling rate, the detailed reaction process cannot be trapped by in situ/ex situ characterizations because of the short reaction time and higher reaction temperature. Therefore, it is urgent to develop characterizations to investigate the reaction mechanism.

(5) The synergistic interplay between dynamic Joule heating and carbothermal shock mechanisms may govern the structural evolution of insulating or low-conductivity materials (Figure 16). Blending materials with carbon additives establishes conductive networks, enabling effective Joule heating. Carbon components undergo instantaneous Joule heating while simultaneously transferring thermal energy to the precursors through carbothermal shock interactions. Additionally, precursors positioned on carbon paper or between graphite plates utilize partially carbonized precursors from initial carbothermal reactions as conductive pathways. This self-generated conductive network subsequently facilitates Joule heating similar to that observed in the blending materials system. Both methodologies combine direct Joule heating with secondary carbothermal effects through dynamic reaction pathways. This dual activation mechanism, where rapid electrical Joule heating couples with carbothermal shock, may constitute the primary driver of structural transformations in these systems.

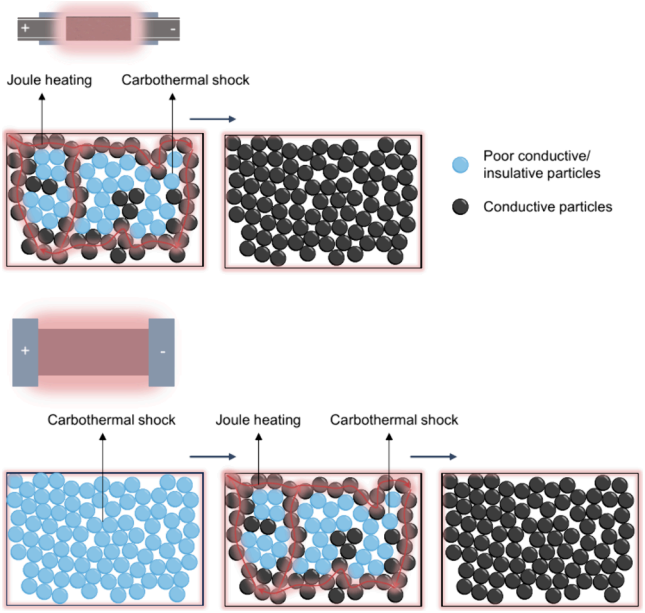

Figure 16. Double effect of Joule heating and carbothermal shock in the UTS process.

The development of advanced energy materials has put forward higher requirements for the preparation and recycling technology. Ultrafast thermal engineering has created excellent opportunities for synthesizing and rejuvenating various functional materials and has shown tremendous potential in the development of energy materials. Especially, opportunities lie in coupling UTS with artificial intelligence (AI)-driven process optimization and renewable energy sources, potentially revolutionizing sustainable manufacturing paradigms for next-generation energy systems. Addressing these challenges will require interdisciplinary efforts in materials engineering, reactor design, and circular economy integration, which will be conducive to providing confidence for industry to better adapt this method toward greater productivity.

AUTHOR INFORMATION

Corresponding Authors

Xingqiao Wu − *Institute for Carbon Neutralization Technology, College of Chemistry and Materials Engineering, Wenzhou University, Wenzhou, Zhejiang 325035, China; Wenzhou Key Laboratory of Sodium-Ion Batteries, Wenzhou University Technology Innovation Institute for Carbon Neutralization, Wenzhou, Zhejiang 325035, China;* orcid.org/0000-0002-3140-6981; Email: xingqiaowu@wzu.edu.cn

Hua Kun Liu − *Institute of Energy Materials Science (IEMS), University of Shanghai for Science and Technology, Shanghai 200093, China*; Email: hua@usst.edu.cn

Minghong Wu − *Key Laboratory of Organic Compound Pollution Control Engineering (MOE), School of*

https://doi.org/10.1021/acsnano.5c04768
ACS Nano XXXX, XXX, XXX−XXX

Environmental and Chemical Engineering, Shanghai University, Shanghai 200444, China; College of Environment & Safety Engineering, Fuzhou University, Fuzhou 350108, China; orcid.org/0000-0002-9776-671X; Email: mhwu@shu.edu.cn

Shulei Chou − *Institute for Carbon Neutralization Technology, College of Chemistry and Materials Engineering, Wenzhou University, Wenzhou, Zhejiang 325035, China; Wenzhou Key Laboratory of Sodium-Ion Batteries, Wenzhou University Technology Innovation Institute for Carbon Neutralization, Wenzhou, Zhejiang 325035, China;* orcid.org/0000-0003-1155-6082; Email: chou@wzu.edu.cn

Authors

Pandeng Zhao − *Institute of Energy Materials Science (IEMS), University of Shanghai for Science and Technology, Shanghai 200093, China; Institute for Carbon Neutralization Technology, College of Chemistry and Materials Engineering, Wenzhou University, Wenzhou, Zhejiang 325035, China; Wenzhou Key Laboratory of Sodium-Ion Batteries, Wenzhou University Technology Innovation Institute for Carbon Neutralization, Wenzhou, Zhejiang 325035, China;* orcid.org/0009-0008-8258-6813

Yinghao Zhang − *Institute for Carbon Neutralization Technology, College of Chemistry and Materials Engineering, Wenzhou University, Wenzhou, Zhejiang 325035, China; Wenzhou Key Laboratory of Sodium-Ion Batteries, Wenzhou University Technology Innovation Institute for Carbon Neutralization, Wenzhou, Zhejiang 325035, China*

Wenjie Huang − *Institute for Carbon Neutralization Technology, College of Chemistry and Materials Engineering, Wenzhou University, Wenzhou, Zhejiang 325035, China; Wenzhou Key Laboratory of Sodium-Ion Batteries, Wenzhou University Technology Innovation Institute for Carbon Neutralization, Wenzhou, Zhejiang 325035, China*

Yuhai Dou − *Institute of Energy Materials Science (IEMS), University of Shanghai for Science and Technology, Shanghai 200093, China*

Shixue Dou − *Institute of Energy Materials Science (IEMS), University of Shanghai for Science and Technology, Shanghai 200093, China*

Complete contact information is available at: https://pubs.acs.org/10.1021/acsnano.5c04768

Notes

The authors declare no competing financial interest.

ACKNOWLEDGMENTS

This work was supported by the National Natural Science Foundation of China (52402302, 52250710680), Postdoctoral Fellowship Programs of CPSF under Grant Number GZC20241072, High-end Foreign Experts Recruitment Plan of China (G2023016009L), Zhejiang Provincial Natural Science Foundation of China (LQ24E020001), Key Research and Development Program of Zhejiang Province (2024C01057, 2023C01232), and Basic Research Project of WenZhou City (G2023016).

VOCABULARY

Ultrahigh temperature shock, a heating method based on the Joule heating effect provides ultrahigh temperature conditions and ultrafast heating/cooling rate; **Joule heating shock**, electric current flows across the reactants and directly converts into thermal energy; **Carbothermal shock**, the conductive substrate acts as the heater on the reactants; **Nonequilibrium thermodynamics**, a branch of thermodynamics studies some systems that are not in thermodynamic equilibrium; **Energy materials**, a series of related energy materials include but not limited to batteries' electrodes, electrolytes, current collectors, and catalysts

REFERENCES

(1) Yao, Y.; Huang, Z.; Xie, P.; Lacey, S. D.; Jacob, R. J.; Xie, H.; Chen, F.; Nie, A.; Pu, T.; Rehwoldt, M.; et al. Carbothermal shock synthesis of high-entropy-alloy nanoparticles. *Science* **2018**, *359* (6383), 1489−1494.

(2) Luong, D. X.; Bets, K. V.; Algozeeb, W. A.; Stanford, M. G.; Kittrell, C.; Chen, W.; Salvatierra, R. V.; Ren, M.; McHugh, E. A.; Advincula, P. A.; et al. Gram-scale bottom-up flash graphene synthesis. *Nature* **2020**, *577* (7792), 647−651.

(3) Dong, Q.; Yao, Y.; Cheng, S.; Alexopoulos, K.; Gao, J.; Srinivas, S.; Wang, Y.; Pei, Y.; Zheng, C.; Brozena, A. H.; et al. Programmable heating and quenching for efficient thermochemical synthesis. *Nature* **2022**, *605* (7910), 470−476.

(4) Murakami, R. K.; Villas-Boas, V. Nanocrystalline magnetic materials obtained by flash annealing. *Mater. Res.* **1999**, *2*, 67−73.

(5) Song, T.-B.; Chen, Y.; Chung, C.-H.; Yang, Y.; Bob, B.; Duan, H.-S.; Li, G.; Tu, K.-N.; Huang, Y.; Yang, Y. Nanoscale joule heating and electromigration enhanced ripening of silver nanowire contacts. *ACS Nano* **2014**, *8* (3), 2804−2811.

(6) Chen, W.; Cheng, Y.; Chen, J.; Bets, K. V.; Salvatierra, R. V.; Ge, C.; Li, J. T.; Luong, D. X.; Kittrell, C.; Wang, Z.; et al. Nondestructive flash cathode recycling. *Nat. Commun.* **2024**, *15* (1), 6250.

(7) Jin, C.; Suenaga, K.; Iijima, S. Plumbing carbon nanotubes. *Nat. Nanotechnol.* **2008**, *3* (1), 17−21.

(8) Bao, W.; Pickel, A. D.; Zhang, Q.; Chen, Y.; Yao, Y.; Wan, J.; Fu, K. K.; Wang, Y.; Dai, J.; Zhu, H.; et al. Flexible, High Temperature, Planar Lighting with Large Scale Printable Nanocarbon Paper. *Adv. Mater.* **2016**, *28* (23), 4684−4691.

(9) Dong, Q.; Lele, A. D.; Zhao, X.; Li, S.; Cheng, S.; Wang, Y.; Cui, M.; Guo, M.; Brozena, A. H.; Lin, Y.; et al. Depolymerization of plastics by means of electrified spatiotemporal heating. *Nature* **2023**, *616* (7957), 488−494.

(10) Yu, Y.; Qin, Z.; Zhang, X.; Chen, Y.; Qin, G.; Li, S. Far-From-Equilibrium Processing Opens Kinetic Paths for Engineering Novel Materials by Breaking Thermodynamic Limits. *ACS Mater. Lett.* **2025**, *7* (1), 319−332.

(11) Yang, Y.; Ghildiyal, P.; Zachariah, M. R. Thermal Shock Synthesis of Metal Nanoclusters within On-the-Fly Graphene Particles. *Langmuir* **2019**, *35* (9), 3413−3420.

(12) Chen, W.; Li, J. T.; Ge, C.; Yuan, Z.; Algozeeb, W. A.; Advincula, P. A.; Gao, G.; Chen, J.; Ling, K.; Choi, C. H.; et al. Turbostratic Boron-Carbon-Nitrogen and Boron Nitride by Flash Joule Heating. *Adv. Mater.* **2022**, *34* (33), No. e2202666.

(13) Yang, C.; Ko, B. H.; Hwang, S.; Liu, Z.; Yao, Y.; Luc, W.; Cui, M.; Malkani, A. S.; Li, T.; Wang, X.; et al. Overcoming immiscibility toward bimetallic catalyst library. *Sci. Adv.* **2020**, *6* (17), No. eaaz6844.

(14) Advincula, P. A.; Beckham, J. L.; Choi, C. H.; Chen, W.; Han, Y.; Kosynkin, D. V.; Lathem, A.; Mayoral, A.; Yacaman, M. J.; Tour, J. M. Tunable Hybridized Morphologies Obtained through Flash Joule Heating of Carbon Nanotubes. *ACS Nano* **2023**, *17* (3), 2506−2516.

(15) Deng, B.; Wang, Z.; Choi, C. H.; Li, G.; Yuan, Z.; Chen, J.; Luong, D. X.; Eddy, L.; Shin, B.; Lathem, A.; et al. Kinetically Controlled Synthesis of Metallic Glass Nanoparticles with Expanded Composition Space. *Adv. Mater.* **2024**, *36* (15), No. 2309956.

(16) Li, Y.; Chen, Y.; Nie, A.; Lu, A.; Jacob, R. J.; Gao, T.; Song, J.; Dai, J.; Wan, J.; Pastel, G.; et al. In Situ, Fast, High-Temperature Synthesis of Nickel Nanoparticles in Reduced Graphene Oxide Matrix. *Adv. Energy Mater.* **2017**, *7* (11), No. 1601783.

(17) Wyss, K. M.; Luong, D. X.; Tour, J. M. Large-Scale Syntheses of 2D Materials: Flash Joule Heating and Other Methods. *Adv. Mater.* **2022**, *34* (8), No. e2106970.
(18) Chen, F.; Yao, Y.; Nie, A.; Xu, S.; Dai, J.; Hitz, E.; Li, Y.; Lu, A.; Huang, Z.; Li, T.; et al. High-Temperature Atomic Mixing toward Well-Dispersed Bimetallic Electrocatalysts. *Adv. Energy Mater.* **2018**, *8* (25), No. 1800466.
(19) Chen, Y.; Xu, S.; Li, Y.; Jacob, R. J.; Kuang, Y.; Liu, B.; Wang, Y.; Pastel, G.; Salamanca-Riba, L. G.; Zachariah, M. R.; et al. FeS_2 Nanoparticles Embedded in Reduced Graphene Oxide toward Robust, High-Performance Electrocatalysts. *Adv. Energy Mater.* **2017**, *7* (19), No. 1700482.
(20) Wyss, K. M.; Chen, W.; Beckham, J. L.; Savas, P. E.; Tour, J. M. Holey and Wrinkled Flash Graphene from Mixed Plastic Waste. *ACS Nano* **2022**, *16* (5), 7804−7815.
(21) Liu, B.; Fu, K.; Gong, Y.; Yang, C.; Yao, Y.; Wang, Y.; Wang, C.; Kuang, Y.; Pastel, G.; Xie, H.; et al. Rapid Thermal Annealing of Cathode-Garnet Interface toward High-Temperature Solid State Batteries. *Nano Lett.* **2017**, *17* (8), 4917−4923.
(22) Wang, C.; Ping, W.; Bai, Q.; Cui, H.; Hensleigh, R.; Wang, R.; Brozena, A. H.; Xu, Z.; Dai, J.; Pei, Y.; et al. A general method to synthesize and sinter bulk ceramics in seconds. *Science* **2020**, *368* (6490), 521−526.
(23) Liu, Y.; Li, P.; Wang, F.; Fang, W.; Xu, Z.; Gao, W.; Gao, C. Rapid roll-to-roll production of graphene films using intensive Joule heating. *Carbon* **2019**, *155*, 462−468.
(24) Cheng, T.; Ma, Z.; Qian, R.; Wang, Y.; Cheng, Q.; Lyu, Y.; Nie, A.; Guo, B. Achieving Stable Cycling of $LiCoO_2$ at 4.6 V by Multilayer Surface Modification. *Adv. Funct. Mater.* **2021**, *31* (2), No. 2001974.
(25) Zhu, W.; Zhang, J.; Luo, J.; Zeng, C.; Su, H.; Zhang, J.; Liu, R.; Hu, E.; Liu, Y.; Liu, W. D.; et al. Ultrafast Non-Equilibrium Synthesis of Cathode Materials for Li-Ion Batteries. *Adv. Mater.* **2023**, *35* (2), No. e2208974.
(26) Qiu, B.; Zhang, M.; Wu, L.; Wang, J.; Xia, Y.; Qian, D.; Liu, H.; Hy, S.; Chen, Y.; An, K.; et al. Gas-solid interfacial modification of oxygen activity in layered oxide cathodes for lithium-ion batteries. *Nat. Commun.* **2016**, *7*, 12108.
(27) Wang, D.; Gao, C.; Zhou, X.; Peng, S.; Tang, M.; Wang, Y.; Huang, L.; Yang, W.; Gao, X. Enhancing reversibility of $LiNi_{0.5}Mn_{1.5}O_4$ by regulating surface oxygen deficiency. *Carbon Energy* **2023**, *5* (11), No. e338.
(28) Xu, B.; Fell, C. R.; Chi, M.; Meng, Y. S. Identifying surface structural changes in layered Li-excess nickel manganese oxides in high voltage lithium ion batteries: A joint experimental and theoretical study. *Energy Environ. Sci.* **2011**, *4* (6), 2223−2233.
(29) Jiang, H.; Zeng, C.; Zhu, W.; Luo, J.; Liu, Z.; Zhang, J.; Liu, R.; Xu, Y.; Chen, Y.; Hu, W. Boosting cycling stability by regulating surface oxygen vacancies of LNMO by rapid calcination. *Nano Res.* **2024**, *17* (4), 2671−2677.
(30) Huang, H.; Zhang, L.; Tian, H.; Yan, J.; Tong, J.; Liu, X.; Zhang, H.; Huang, H.; Hao, S. m.; Gao, J.; et al. Pulse High Temperature Sintering to Prepare Single-Crystal High Nickel Oxide Cathodes with Enhanced Electrochemical Performance. *Adv. Energy Mater.* **2023**, *13* (3), No. 2203188.
(31) Zhu, W.; Su, H.; Bai, P.; Li, Z.; Zhang, J.; Zhang, J.; Li, M.; Chen, Y.; Xu, Y. A layered/spinel heterostructured cathode for Li-ion batteries prepared by ultrafast Joule heating. *Chem. Eng. J.* **2024**, *480*, No. 148045.
(32) Luan, C.; Jiang, L.; Zheng, X.; Cao, Y.; Huang, Z.; Lu, Q.; Li, J.; Wang, Y.; Deng, Y.; Rogach, A. L. Direct observation of the ultrafast formation of cation-disordered rocksalt oxides as regenerable cathodes for lithium-ion batteries. *Chem. Eng. J.* **2023**, *462*, No. 142180.
(33) Li, Z.; Huang, P.; Zhang, J.; Guo, Z.; Liu, Z.; Chen, L.; Zhang, J.; Luo, J.; Tao, X.; Miao, Z.; et al. Ultra-uniform interfacial matrix via high-temperature thermal shock for long-cycle stability cathodes of sodium-ion batteries. *Energy Environ. Sci.* **2025**, *18* (6), 2962−2972.
(34) Yang, Y.; Wu, C.; He, X. X.; Zhao, J.; Yang, Z.; Li, L.; Wu, X.; Li, L.; Chou, S. L. Boosting the Development of Hard Carbon for Sodium-Ion Batteries: Strategies to Optimize the Initial Coulombic Efficiency. *Adv. Funct. Mater.* **2024**, *34*, No. 2302277.
(35) Wu, C.; Yang, Y.; Zhang, Y.; Xu, H.; He, X.; Wu, X.; Chou, S. Hard carbon for sodium-ion batteries: progress, strategies and future perspective. *Chem. Sci.* **2024**, *15* (17), 6244−6268.
(36) He, X. X.; Lai, W. H.; Liang, Y.; Zhao, J. H.; Yang, Z.; Peng, J.; Liu, X. H.; Wang, Y. X.; Qiao, Y.; Li, L.; et al. Achieving All-Plateau and High-Capacity Sodium Insertion in Topological Graphitized Carbon. *Adv. Mater.* **2023**, *35* (40), No. 2302613.
(37) Xiong, J.; Wang, Y.; Lu, J.; Xi, F.; Tong, Z.; Ma, W.; Li, S. Upcycling of photovoltaic waste graphite into high performance graphite anode. *J. Colloid Interface Sci.* **2025**, *685*, 555−564.
(38) Baskar, A. V.; Singh, G.; Ruban, A. M.; Davidraj, J. M.; Bahadur, R.; Sooriyakumar, P.; Kumar, P.; Karakoti, A.; Yi, J.; Vinu, A. Recent Progress in Synthesis and Application of Biomass-Based Hybrid Electrodes for Rechargeable Batteries. *Adv. Funct. Mater.* **2023**, *33* (3), No. 2208349.
(39) Chen, C.; Chen, Y.; Zhu, S.; Dai, J.; Pastel, G.; Yao, Y.; Liu, D.; Wang, Y.; Wan, J.; Li, T.; et al. Catalyst-Free In Situ Carbon Nanotube Growth in Confined Space via High Temperature Gradient. *Research (Wash D C)* **2018**, *2018*, No. 1793784.
(40) Zhang, F.; Yao, Y.; Wan, J.; Henderson, D.; Zhang, X.; Hu, L. High Temperature Carbonized Grass as a High Performance Sodium Ion Battery Anode. *ACS Appl. Mater. Interfaces* **2017**, *9* (1), 391−397.
(41) Lege, N.; Zhang, Y.; Lai, W.; He, X.; Wang, Y.-X.; Zhao, L.; Liu, M.; Wu, X.; Chou, S. Potassium-Escaping Balances Degree of Graphitization and Pore Channel Structure in Hard Carbon to Boost Plateau Sodium Storage Capacity. *Chem. Sci.* **2025**, *16* (3), 1179−1188.
(42) Wu, C.; Huang, W.; Zhang, Y.; Chen, Q.; Li, L.; Zhang, Y.; Wu, X.; Chou, S. Revisiting the Critical Role of Metallic Ash Elements in the Development of Hard Carbon for Advancing Sodium-Ion Battery Applications. *eScience* **2025**, No. 100371.
(43) Dong, S.; Song, Y.; Fang, Y.; Wang, G.; Gao, Y.; Zhu, K.; Cao, D. Rapid Carbonization of Anthracite Coal via Flash Joule Heating for Sodium Ion Storage. *ACS Appl. Energy Mater.* **2024**, *7* (24), 11288−11296.
(44) Lyu, T.; Liang, L.; Liu, K.; Luo, F.; Fan, Q.; Guo, P.; Wang, D.; Wei, G.; Tao, L.; Zheng, Z. Graphitized Layers Encapsulated Carbon Nanofibers as Li-Free Anode for Hybrid Li-Ion/Metal Batteries. *Small* **2025**, *21* (10), No. e2412457.
(45) Lyu, T.; Huang, M.; Xu, J.; Lin, X.; Xiao, X.; Liang, L.; Zhang, C.; Wang, D.; Zheng, Z. Interfacial Chemistry and Lithiophilicity Design for High Energy Hybrid Li-Ion/Metal Batteries in a Wide Temperature Range. *Adv. Funct. Mater.* **2025**, No. 2500212.
(46) Zhu, G. L.; Zhao, C. Z.; Huang, J. Q.; He, C.; Zhang, J.; Chen, S.; Xu, L.; Yuan, H.; Zhang, Q. Fast Charging Lithium Batteries: Recent Progress and Future Prospects. *Small* **2019**, *15* (15), No. e1805389.
(47) Huang, P.; Li, Z.; Chen, L.; Li, Y.; Liu, Z.; Zhang, J.; Luo, J.; Zhang, W.; Liu, W. D.; Zhang, X.; et al. Ultrafast Dual-Shock Chemistry Synthesis of Ordered/Disordered Hybrid Carbon Anodes: High-Rate Performance of Li-Ion Batteries. *ACS Nano* **2024**, *18* (28), 18344−18354.
(48) Yang, H.; Sun, L.; Zhai, S.; Wang, X.; Liu, C.; Wu, H.; Deng, W. Ordered-Range Tuning of Flash Graphene for Fast-Charging Lithium-Ion Batteries. *ACS Appl. Nano Mater.* **2023**, *6* (4), 2450−2458.
(49) Wu, X.; Li, Z.; Feng, W.; Luo, W.; Liao, L.; Cai, H.; Chen, X.; Deng, Z.; Wu, J.; Xing, B.; et al. Insights into electrolyte-induced temporal and spatial evolution of an ultrafast-charging Bi-based anode for sodium-ion batteries. *Energy Storage Mater.* **2024**, *66*, No. 103219.
(50) Lu, J.; Liu, S.; Liu, J.; Qian, G.; Wang, D.; Gong, X.; Deng, Y.; Chen, Y.; Wang, Z. Millisecond Conversion of Photovoltaic Silicon Waste to Binder-Free High Silicon Content Nanowires Electrodes. *Adv. Energy Mater.* **2021**, *11* (40), No. 2102103.
(51) Chen, Y.; Li, Y.; Wang, Y.; Fu, K.; Danner, V. A.; Dai, J.; Lacey, S. D.; Yao, Y.; Hu, L. Rapid, in Situ Synthesis of High Capacity

https://doi.org/10.1021/acsnano.5c04768
ACS Nano XXXX, XXX, XXX−XXX

Battery Anodes through High Temperature Radiation-Based Thermal Shock. *Nano Lett.* **2016**, *16* (9), 5553−5558.
(52) Cheng, Y.; Chen, J.; Deng, B.; Chen, W.; Silva, K. J.; Eddy, L.; Wu, G.; Chen, Y.; Li, B.; Kittrell, C.; et al. Flash upcycling of waste glass fibre-reinforced plastics to silicon carbide. *Nat. Sustainability* **2024**, *7* (4), 452−462.
(53) Yu, L.; Zeng, K.; Li, C.; Lin, X.; Liu, H.; Shi, W.; Qiu, H. J.; Yuan, Y.; Yao, Y. High-entropy alloy catalysts: From bulk to nano toward highly efficient carbon and nitrogen catalysis. *Carbon Energy* **2022**, *4* (5), 731−761.
(54) Liu, S.; Liu, B.; Liu, M.; Xiong, J.; Gao, Y.; Wang, B.; Hu, Y. Rapid, in situ synthesis of ultra-small silicon particles for boosted lithium storage capability through ultrafast Joule heating. *Nanoscale* **2024**, *16* (5), 2531−2539.
(55) Dong, Q.; Hong, M.; Gao, J.; Li, T.; Cui, M.; Li, S.; Qiao, H.; Brozena, A. H.; Yao, Y.; Wang, X.; et al. Rapid Synthesis of High-Entropy Oxide Microparticles. *Small* **2022**, *18* (11), No. e2104761.
(56) Liu, Y.; Tian, X.; Han, Y.-C.; Chen, Y.; Hu, W. High-temperature shock synthesis of high-entropy-alloy nanoparticles for catalysis. *Chin. J. Catal.* **2023**, *48*, 66−89.
(57) Ren, R.; Xiong, Y.; Xu, Z.; Zhang, J.; Zhang, Y.; Zhu, G.; Yin, K.; Dong, S. Fast synthesis of high-entropy oxides for lithium-ion storage. *Chem. Eng. J.* **2024**, *479*, No. 147896.
(58) Ren, R.; Wu, D.; Zhang, J.; You, X.; Xu, Z.; Yang, J.; Ren, H.; Zhu, G.; Zhang, Y.; Dong, S. Synthesis of spinel $(Mg_{0.2}Co_{0.2}Ni_{0.2}Cu_{0.2}Zn_{0.2})Fe_2O_4$ in seconds for lithium-ion battery anodes. *J. Mater. Chem. A* **2024**, *12* (6), 3251−3257.
(59) Zhou, R.; Meng, C.; Zhu, F.; Li, Q.; Liu, C.; Fan, S.; Jiang, K. High-performance supercapacitors using a nanoporous current collector made from super-aligned carbon nanotubes. *Nanotechnology* **2010**, *21* (34), No. 345701.
(60) Park, S.; Shim, H.-W.; Lee, C. W.; Song, H. J.; Park, I. J.; Kim, J.-C.; Hong, K. S.; Kim, D.-W. Tailoring uniform γ-MnO_2 nanosheets on highly conductive three-dimensional current collectors for high-performance supercapacitor electrodes. *Nano Res.* **2015**, *8* (3), 990−1004.
(61) Yazici, M. S.; Krassowski, D.; Prakash, J. Flexible graphite as battery anode and current collector. *J. Power Sources* **2005**, *141* (1), 171−176.
(62) Hu, L.; Wu, H.; La Mantia, F.; Yang, Y.; Cui, Y. Thin, flexible secondary Li-ion paper batteries. *ACS Nano* **2010**, *4* (10), 5843−5848.
(63) Krasheninnikov, A.; Banhart, F. Engineering of nanostructured carbon materials with electron or ion beams. *Nat. Mater.* **2007**, *6* (10), 723−733.
(64) Kis, A.; Csanyi, G.; Salvetat, J.-P.; Lee, T.-N.; Couteau, E.; Kulik, A.; Benoit, W.; Brugger, J.; Forro, L. Reinforcement of single-walled carbon nanotube bundles by intertube bridging. *Nat. Mater.* **2004**, *3* (3), 153−157.
(65) Terrones, M.; Banhart, F.; Grobert, N.; Charlier, J.-C.; Terrones, H.; Ajayan, P. Molecular junctions by joining single-walled carbon nanotubes. *Phys. Rev. Lett.* **2002**, *89* (7), No. 075505.
(66) Li, R.; Gong, W.; He, Q.; Li, Q.; Lu, W.; Zhu, W. Joining cross-stacked carbon nanotube architecture with covalent bonding. *Appl. Phys. Lett.* **2017**, *110* (18), No. 183101.
(67) Pashkin, E.; Pankov, A.; Kulnitskiy, B.; Perezhogin, I.; Karaeva, A.; Mordkovich, V.; Popov, M. Y.; Sorokin, P.; Blank, V. The unexpected stability of multiwall nanotubes under high pressure and shear deformation. *Appl. Phys. Lett.* **2016**, *109* (8), No. 081904.
(68) Yao, Y.; Fu, K. K.; Zhu, S.; Dai, J.; Wang, Y.; Pastel, G.; Chen, Y.; Li, T.; Wang, C.; Li, T.; et al. Carbon Welding by Ultrafast Joule Heating. *Nano Lett.* **2016**, *16* (11), 7282−7289.
(69) Romo-Herrera, J.; Terrones, M.; Terrones, H.; Dag, S.; Meunier, V. Covalent 2D and 3D networks from 1D nanostructures: designing new materials. *Nano Lett.* **2007**, *7* (3), 570−576.
(70) Savvatimskiy, A. Measurements of the melting point of graphite and the properties of liquid carbon (a review for 1963−2003). *Carbon* **2005**, *43* (6), 1115−1142.
(71) Yao, Y.; Jiang, F.; Yang, C.; Fu, K. K.; Hayden, J.; Lin, C. F.; Xie, H.; Jiao, M.; Yang, C.; Wang, Y.; et al. Epitaxial Welding of Carbon Nanotube Networks for Aqueous Battery Current Collectors. *ACS Nano* **2018**, *12* (6), 5266−5273.
(72) Chen, Y.; Fu, K.; Zhu, S.; Luo, W.; Wang, Y.; Li, Y.; Hitz, E.; Yao, Y.; Dai, J.; Wan, J.; et al. Reduced Graphene Oxide Films with Ultrahigh Conductivity as Li-Ion Battery Current Collectors. *Nano Lett.* **2016**, *16* (6), 3616−3623.
(73) Liu, S.; Wang, P.; Liu, C.; Deng, Y.; Dou, S.; Liu, Y.; Xu, J.; Wang, Y.; Liu, W.; Hu, W.; et al. Nanomanufacturing of RGO-CNT Hybrid Film for Flexible Aqueous Al-Ion Batteries. *Small* **2020**, *16* (37), No. e2002856.
(74) Yang, C.; Wu, Q.; Xie, W.; Zhang, X.; Brozena, A.; Zheng, J.; Garaga, M. N.; Ko, B. H.; Mao, Y.; He, S.; et al. Copper-coordinated cellulose ion conductors for solid-state batteries. *Nature* **2021**, *598* (7882), 590−596.
(75) Okur, F.; Zhang, H.; Baumgartner, J. F.; Sivavec, J.; Klimpel, M.; Wasser, G. P.; Dubey, R.; Jeurgens, L. P. H.; Chernyshov, D.; van Beek, W.; et al. Ultrafast Sintering of Dense $Li_7La_3Zr_2O_{12}$ Membranes for Li Metal All-Solid-State Batteries. *Adv. Sci. (Weinh)* **2025**, *12*, No. e2412370.
(76) Hong, M.; Dong, Q.; Xie, H.; Clifford, B. C.; Qian, J.; Wang, X.; Luo, J.; Hu, L. Ultrafast Sintering of Solid-State Electrolytes with Volatile Fillers. *ACS Energy Lett.* **2021**, *6* (11), 3753−3760.
(77) Hong, M.; Dong, Q.; Xie, H.; Wang, X.; Brozena, A. H.; Gao, J.; Wang, C.; Chen, C.; Rao, J.; Luo, J.; et al. Tailoring grain growth and densification toward a high-performance solid-state electrolyte membrane. *Mater. Today* **2021**, *42*, 41−48.
(78) Wang, R.; Ping, W.; Wang, C.; Liu, Y.; Gao, J.; Dong, Q.; Wang, X.; Mo, Y.; Hu, L. Computation-Guided Synthesis of New Garnet-Type Solid-State Electrolytes via an Ultrafast Sintering Technique. *Adv. Mater.* **2020**, *32* (46), No. 2005059.
(79) Wang, C.; Xie, H.; Ping, W.; Dai, J.; Feng, G.; Yao, Y.; He, S.; Weaver, J.; Wang, H.; Gaskell, K.; et al. A general, highly efficient, high temperature thermal pulse toward high performance solid state electrolyte. *Energy Storage Mater.* **2019**, *17*, 234−241.
(80) Xiang, W.; Ma, R.; Liu, X.; Kong, X.; Shen, S.; Wang, L.; Jin, Z.; Zhan, Z.; Chen, C.; Wang, C. Rapid Li compensation toward highly conductive solid state electrolyte film. *Nano Energy* **2023**, *116*, No. 108816.
(81) Chen, L.; Huang, X.; Ma, R.; Xiang, W.; Ma, J.; Wu, Y.; Yang, D.; Wang, C.; Ping, W.; Xiang, H. A nanocrystal garnet skeleton-derived high-performance composite solid-state electrolyte membrane. *Energy Storage Mater.* **2024**, *65*, No. 103140.
(82) Chen, S.; Nie, L.; Hu, X.; Zhang, Y.; Zhang, Y.; Yu, Y.; Liu, W. Ultrafast Sintering for Ceramic-Based All-Solid-State Lithium-Metal Batteries. *Adv. Mater.* **2022**, *34* (33), No. e2200430.
(83) Yao, X.; Chen, S.; Wang, C.; Chen, T.; Li, J.; Xue, S.; Deng, Z.; Zhao, W.; Nan, B.; Zhao, Y.; et al. Interface Welding via Thermal Pulse Sintering to Enable 4.6 V Solid-State Batteries. *Adv. Energy Mater.* **2024**, *14* (10), No. 2303422.
(84) Feng, Y.; Yang, L.; Yan, Z.; Zuo, D.; Zhu, Z.; Zeng, L.; Zhu, Y.; Wan, J. Discovery of high entropy garnet solid-state electrolytes via ultrafast synthesis. *Energy Storage Mater.* **2023**, *63*, No. 103053.
(85) Wu, X.; Chen, X.; Li, X.; Yan, Y.; Huang, J.; Li, J.; Shen, R.; Tian, H.; Yang, D.; Zhang, H. A unique ligand effect in Pt-based core−shell nanocubes to boost oxygen reduction electrocatalysis. *J. Mater. Chem. A* **2021**, *9* (39), 22653−22659.
(86) Li, J.; Ji, L.; Li, X.; Luo, S.; Zhao, P.; Wu, X.; Zhang, H.; Yang, D. Synergistic multiple effects by de-alloyed strategy for efficient and durable oxygen reduction. *J. Power Sources* **2025**, *629*, No. 236052.
(87) Wu, X.; Jiang, Y.; Yan, Y.; Li, X.; Luo, S.; Huang, J.; Li, J.; Shen, R.; Yang, D.; Zhang, H. Tuning Surface Structure of Pd_3Pb/Pt_nPb Nanocrystals for Boosting the Methanol Oxidation Reaction. *Adv. Sci. (Weinh)* **2019**, *6* (24), No. 1902249.
(88) Li, C.; Wang, Z.; Liu, M.; Wang, E.; Wang, B.; Xu, L.; Jiang, K.; Fan, S.; Sun, Y.; Li, J.; et al. Ultrafast self-heating synthesis of robust heterogeneous nanocarbides for high current density hydrogen evolution reaction. *Nat. Commun.* **2022**, *13* (1), 3338.

https://doi.org/10.1021/acsnano.5c04768
ACS Nano XXXX, XXX, XXX−XXX

(89) Deng, B.; Wang, Z.; Chen, W.; Li, J. T.; Luong, D. X.; Carter, R. A.; Gao, G.; Yakobson, B. I.; Zhao, Y.; Tour, J. M. Phase controlled synthesis of transition metal carbide nanocrystals by ultrafast flash Joule heating. *Nat. Commun.* **2022**, *13* (1), 262.
(90) Wan, C.; Regmi, Y. N.; Leonard, B. M. Multiple Phases of Molybdenum Carbide as Electrocatalysts for the Hydrogen Evolution Reaction. *Angew. Chem.* **2014**, *126* (25), 6525−6528.
(91) Sun, J.; Ren, G.; Qin, S.; Zhao, Z.; Li, Z.; Zhang, Z.; Li, C.; Meng, X. Reconstruction Co-O-Mo in amorphous-crystalline MoO_x/$Co(OH)_2$ interface for industry-level active and stable electrocatalytic seawater hydrogen evolution. *Nano Energy* **2024**, *121*, No. 109246.
(92) Sun, J.; Qin, S.; Zhao, Z.; Zhang, Z.; Meng, X. Rapid carbothermal shocking fabrication of iron-incorporated molybdenum oxide with heterogeneous spin states for enhanced overall water/seawater splitting. *Mater. Horiz.* **2024**, *11* (5), 1199−1211.
(93) Zhao, Z.; Sun, J.; Li, Z.; Xu, X.; Zhang, Z.; Li, C.; Wang, L.; Meng, X. Rapid synthesis of efficient Mo-based electrocatalyst for the hydrogen evolution reaction in alkaline seawater with 11.28% solar-to-hydrogen efficiency. *J. Mater. Chem. A* **2023**, *11* (19), 10346−10359.
(94) Sun, J.; Qin, S.; Zhang, Z.; Li, C.; Xu, X.; Li, Z.; Meng, X. Joule heating synthesis of well lattice-matched $Co_2Mo_3O_8$/MoO_2 heterointerfaces with greatly improved hydrogen evolution reaction in alkaline seawater electrolysis with 12.4% STH efficiency. *Appl. Catal., B* **2023**, *338*, 123015.
(95) Zhao, Z.; Sun, J.; Li, X.; Zhang, Z.; Meng, X. Joule heating synthesis of NiFe alloy/MoO2 and in-situ transformed (Ni,Fe)OOH/MoO_2 heterostructure as effective complementary electrocatalysts for overall splitting in alkaline seawater. *Appl. Catal., B* **2024**, *340*, No. 123277.
(96) Liu, S.; Hu, Z.; Wu, Y.; Zhang, J.; Zhang, Y.; Cui, B.; Liu, C.; Hu, S.; Zhao, N.; Han, X.; et al. Dislocation-Strained IrNi Alloy Nanoparticles Driven by Thermal Shock for the Hydrogen Evolution Reaction. *Adv. Mater.* **2020**, *32* (48), No. e2006034.
(97) Liu, P.; Zhang, X.; Fei, J.; Shi, Y.; Zhu, J.; Zhang, D.; Zhao, L.; Wang, L.; Lai, J. Frank Partial Dislocations in Coplanar Ir/C Ultrathin Nanosheets Boost Hydrogen Evolution Reaction. *Adv. Mater.* **2024**, *36* (11), No. e2310591.
(98) Liu, S.; Shen, Y.; Zhang, Y.; Cui, B.; Xi, S.; Zhang, J.; Xu, L.; Zhu, S.; Chen, Y.; Deng, Y.; et al. Extreme Environmental Thermal Shock Induced Dislocation-Rich Pt Nanoparticles Boosting Hydrogen Evolution Reaction. *Adv. Mater.* **2022**, *34* (2), No. e2106973.
(99) Wang, Y.; Zhang, Y.; Xing, P.; Li, X.; Du, Q.; Fan, X.; Cai, Z.; Yin, R.; Yao, Y.; Gan, W. Self-Encapsulation of High-Entropy Alloy Nanoparticles inside Carbonized Wood for Highly Durable Electrocatalysis. *Adv. Mater.* **2024**, *36* (28), No. e2402391.
(100) Xing, L.; Liu, R.; Gong, Z.; Liu, J.; Liu, J.; Gong, H.; Huang, K.; Fei, H. Ultrafast Joule heating synthesis of hierarchically porous graphene-based Co-N-C single-atom monoliths. *Nano Res.* **2022**, *15* (5), 3913−3919.
(101) Xu, S.; Chen, Y.; Li, Y.; Lu, A.; Yao, Y.; Dai, J.; Wang, Y.; Liu, B.; Lacey, S. D.; Pastel, G. R.; et al. Universal, In Situ Transformation of Bulky Compounds into Nanoscale Catalysts by High-Temperature Pulse. *Nano Lett.* **2017**, *17* (9), 5817−5822.
(102) Li, Y.; Gao, T.; Yao, Y.; Liu, Z.; Kuang, Y.; Chen, C.; Song, J.; Xu, S.; Hitz, E. M.; Liu, B.; et al. In Situ "Chainmail Catalyst" Assembly in Low-Tortuosity, Hierarchical Carbon Frameworks for Efficient and Stable Hydrogen Generation. *Adv. Energy Mater.* **2018**, *8* (25), No. 1801289.
(103) Zhu, S.; Xu, Q.; Guan, C.; Chang, Y.; Han, G.; Deng, B. Confined Flash Pt_1/WC_x inside Carbon Nanotubes for Efficient and Durable Electrocatalysis. *Nano Lett.* **2025**, *25* (8), 3066−3074.
(104) Yang, H.; Zhang, Z.; Wang, Z.; Zhang, F.; Liu, S.; Zhang, L.; Shi, C.; Hou, P. X.; Cheng, H. M.; Wang, X.; et al. Integrated High-Entropy Alloy Nanowire/Carbon Nanotube Membrane Electrode for Efficient Hydrogen Evolution in Acid Solution. *Adv. Funct. Mater.* **2025**, No. 2425156.
(105) Fu, S.; Ma, Y.; Yang, X.; Yao, X.; Jiao, Z.; Cheng, L.; Zhao, P. Defect and interface engineering of hexagonal Fe_2O_3/$ZnCo_2O_4$ n-n heterojunction for efficient oxygen evolution reaction. *Appl. Catal., B* **2023**, *333*, No. 122813.
(106) Wang, X.; Zhao, Y.; Chen, G.; Zhao, X.; Liu, C.; Sridar, S.; Pizano, L. F. L.; Li, S.; Brozena, A. H.; Guo, M.; et al. Ultrahigh-temperature melt printing of multi-principal element alloys. *Nat. Commun.* **2022**, *13* (1), 6724.
(107) Yao, Y.; Huang, Z.; Li, T.; Wang, H.; Liu, Y.; Stein, H. S.; Mao, Y.; Gao, J.; Jiao, M.; Dong, Q.; et al. High-throughput, combinatorial synthesis of multimetallic nanoclusters. *Proc. Natl. Acad. Sci. U. S. A.* **2020**, *117* (12), 6316−6322.
(108) Jung, W. B.; Park, H.; Jang, J. S.; Kim, D. Y.; Kim, D. W.; Lim, E.; Kim, J. Y.; Choi, S.; Suk, J.; Kang, Y.; et al. Polyelemental Nanoparticles as Catalysts for a Li-O_2 Battery. *ACS Nano* **2021**, *15* (3), 4235−4244.
(109) Kuang, G.; Wang, K.; Wang, Y.; Lei, L.; Zhuang, L.; Xu, Z. Joule-Heating-Driven Encapsulation of FeCo Nanoparticles in Ion-Selective Carbon Shell for Stable Seawater Electrolysis. *ChemSusChem* **2025**, No. e202402710.
(110) Li, Y.; Wu, H.; Zhang, J.; Lu, Q.; Han, X.; Zheng, X.; Deng, Y.; Hu, W. Rapid synthesis of doped metal oxidesviaJoule heating for oxygen electrocatalysis regulation. *J. Mater. Chem. A* **2023**, *11* (19), 10267−10276.
(111) Chen, J.; Ma, Y.; Huang, T.; Jiang, T.; Park, S.; Xu, J.; Wang, X.; Peng, Q.; Liu, S.; Wang, G.; et al. Ruthenium-Based Binary Alloy with Oxide Nanosheath for Highly Efficient and Stable Oxygen Evolution Reaction in Acidic Media. *Adv. Mater.* **2024**, *36* (26), No. e2312369.
(112) Yang, C.; Cui, M.; Li, N.; Liu, Z.; Hwang, S.; Xie, H.; Wang, X.; Kuang, Y.; Jiao, M.; Su, D.; et al. In situ iron coating on nanocatalysts for efficient and durable oxygen evolution reaction. *Nano Energy* **2019**, *63*, No. 103855.
(113) Zou, X.; Xie, J.; Mei, Z.; Jing, Q.; Sheng, X.; Zhang, C.; Yang, Y.; Sun, M.; Ren, F.; Wang, L.; et al. High-entropy engineering with regulated defect structure and electron interaction tuning active sites for trifunctional electrocatalysis. *Proc. Natl. Acad. Sci. U.S.A.* **2024**, *121* (13), No. e2313239121.
(114) Chang, R.; Li, H.; Tian, X.; Yang, Y.; Dong, T.; Wang, Z.; Lai, J.; Feng, S.; Wang, L. In Situ, Rapid Synthesis of Carbon-Loaded High Density and Ultrasmall High Entropy Oxide Nanoparticles as Efficient Electrocatalysts. *Small* **2024**, *20*, No. e2309937.
(115) Abdelhafiz, A.; Wang, B.; Harutyunyan, A. R.; Li, J. Carbothermal Shock Synthesis of High Entropy Oxide Catalysts: Dynamic Structural and Chemical Reconstruction Boosting the Catalytic Activity and Stability toward Oxygen Evolution Reaction. *Adv. Energy Mater.* **2022**, *12* (35), No. 2200742.
(116) Cui, M.; Yang, C.; Li, B.; Dong, Q.; Wu, M.; Hwang, S.; Xie, H.; Wang, X.; Wang, G.; Hu, L. High-Entropy Metal Sulfide Nanoparticles Promise High-Performance Oxygen Evolution Reaction. *Adv. Energy Mater.* **2021**, *11* (3), No. 2002887.
(117) Qiao, H.; Wang, X.; Dong, Q.; Zheng, H.; Chen, G.; Hong, M.; Yang, C.-P.; Wu, M.; He, K.; Hu, L. A high-entropy phosphate catalyst for oxygen evolution reaction. *Nano Energy* **2021**, *86*, No. 106029.
(118) Chen, J.; Ma, J.; Huang, T.; Liu, Q.; Liu, X.; Luo, R.; Xu, J.; Wang, X.; Jiang, T.; Liu, H.; et al. Iridium-Free High-Entropy Alloy for Acidic Water Oxidation at High Current Densities. *Angew. Chem., Int. Ed. Engl.* **2025**, No. e202503330.
(119) Liao, W.; Qing, F.; Liu, Q.; Wu, R.; Zhou, C.; Chen, L.; Chen, Y.; Li, X. Carbothermal Shock Synthesis of Lattice Oxygen-Mediated High-Entropy FeCoNiCuMo-O Electrocatalyst with a Fast Kinetic, High Efficiency, and Stable Oxygen Evolution Reaction. *Nano Lett.* **2025**, *25* (4), 1575−1583.
(120) Luo, Q.; Wang, K.; Zhang, Q.; Ding, W.; Wang, R.; Li, L.; Peng, S.; Ji, D.; Qin, X. Tailoring Single-Atom Coordination Environments in Carbon Nanofibers via Flash Heating for Highly Efficient Bifunctional Oxygen Electrocatalysis. *Angew. Chem., Int. Ed. Engl.* **2025**, *64*, No. e202413369.
(121) Li, D.; Zhang, L.; Kuang, L.; Qin, H.; Hu, X.; He, J.; Ni, H.; He, Y. Carbothermal shock synthesis of CoO/N/C nanoparticles with

https://doi.org/10.1021/acsnano.5c04768
ACS Nano XXXX, XXX, XXX−XXX

superior durability for oxygen reduction reaction. *J. Power Sources* **2023**, *587*, No. 233699.
(122) Sheng, X.; Mei, Z.; Jing, Q.; Zou, X.; Wang, L.; Xu, Q.; Guo, H. Revealing the Orbital Interactions between Dissimilar Metal Sites during Oxygen Reduction Process. *Small* **2024**, *20* (7), No. e2305390.
(123) Qin, G.; Sun, S.; Zhang, X.; Han, Z.; Li, Y.; Han, G.; Li, Y.; Zhu, S. Millisecond activity modulation of atomically-dispersed Fe−N−C catalysts. *Energy Storage Mater.* **2024**, *69*, No. 103421.
(124) Lu, Q.; Wu, H.; Zheng, X.; Chen, Y.; Rogach, A. L.; Han, X.; Deng, Y.; Hu, W. Encapsulating Cobalt Nanoparticles in Interconnected N-Doped Hollow Carbon Nanofibers with Enriched Co-N-C Moiety for Enhanced Oxygen Electrocatalysis in Zn-Air Batteries. *Adv. Sci. (Weinh)* **2021**, *8* (20), No. e2101438.
(125) Lai, L.; Ye, S.; Liu, F.; She, F.; Prabowo, J.; Chen, J.; Deng, Y.; Li, H.; Wei, L.; Chen, Y. Carbon catalysts derived from ZIF-8: Joule heating vs. furnace heating. *Carbon* **2025**, *234*, No. 119982.
(126) Shi, W.; Li, Z.; Gong, Z.; Liang, Z.; Liu, H.; Han, Y. C.; Niu, H.; Song, B.; Chi, X.; Zhou, J.; et al. Transient and general synthesis of high-density and ultrasmall nanoparticles on two-dimensional porous carbon via coordinated carbothermal shock. *Nat. Commun.* **2023**, *14* (1), 2294.
(127) Cui, M.; Yang, C.; Hwang, S.; Li, B.; Dong, Q.; Wu, M.; Xie, H.; Wang, X.; Wang, G.; Hu, L. Rapid Atomic Ordering Transformation toward Intermetallic Nanoparticles. *Nano Lett.* **2022**, *22* (1), 255−262.
(128) Yan, W.; Wang, X.; Liu, M.; Ma, K.; Wang, L.; Liu, Q.; Wang, C.; Jiang, X.; Li, H.; Tang, Y.; et al. PCTS-Controlled Synthesis of $L1_0$/$L1_2$-Typed Pt-Mn Intermetallics for Electrocatalytic Oxygen Reduction. *Adv. Funct. Mater.* **2024**, *34* (6), No. 2310487.
(129) Kim, C.; Bui, J. C.; Luo, X.; Cooper, J. K.; Kusoglu, A.; Weber, A. Z.; Bell, A. T. Tailored catalyst microenvironments for CO_2 electroreduction to multicarbon products on copper using bilayer ionomer coatings. *Nat. Energy* **2021**, *6* (11), 1026−1034.
(130) Rooney, C. L.; Lyons, M.; Wu, Y.; Hu, G.; Wang, M.; Choi, C.; Gao, Y.; Chang, C. W.; Brudvig, G. W.; Feng, Z.; et al. Active Sites of Cobalt Phthalocyanine in Electrocatalytic CO_2 Reduction to Methanol. *Angew. Chem., Int. Ed. Engl.* **2024**, *63* (2), No. e202310623.
(131) Bao, Y.; Xiao, J.; Huang, Y.; Li, Y.; Yao, S.; Qiu, M.; Yang, X.; Lei, L.; Li, Z.; Hou, Y.; et al. Regulating Spin Polarization via Axial Nitrogen Traction at Fe-N_5 Sites Enhanced Electrocatalytic CO_2 Reduction for Zn-CO_2 Batteries. *Angew. Chem., Int. Ed. Engl.* **2024**, *63* (43), No. e202406030.
(132) Yang, H.; Guo, N.; Xi, S.; Wu, Y.; Yao, B.; He, Q.; Zhang, C.; Wang, L. Potential-driven structural distortion in cobalt phthalocyanine for electrocatalytic CO_2/CO reduction towards methanol. *Nat. Commun.* **2024**, *15* (1), 7703.
(133) Hu, C.; Hong, X.; Liu, M.; Shen, K.; Chen, L.; Li, Y. Hierarchically Ordered Pore Engineering of Carbon Supports with High-Density Edge-Type Single-Atom Sites to Boost Electrochemical CO_2 Reduction. *Adv. Mater.* **2024**, *36* (48), No. e2409531.
(134) Xi, D.; Li, J.; Low, J.; Mao, K.; Long, R.; Li, J.; Dai, Z.; Shao, T.; Zhong, Y.; Li, Y.; et al. Limiting the Uncoordinated N Species in M−N_x Single-Atom Catalysts toward Electrocatalytic CO_2 Reduction in Broad Voltage Range. *Adv. Mater.* **2022**, *34* (25), No. 2104090.
(135) Wulan, B.; Zhao, L.; Tan, D.; Cao, X.; Ma, J.; Zhang, J. Electrochemically Driven Interfacial Transformation For High-Performing Solar-To-Fuel Electrocatalytic Conversion. *Adv. Energy Mater.* **2022**, *12* (19), No. 2103960.
(136) Chen, X.; Lu, R.; Li, C.; Luo, W.; Yu, R.; Zhu, J.; Lv, L.; Dai, Y.; Gong, S.; Zhou, Y.; et al. Activating inert non-defect sites in Bi catalysts using tensile strain engineering for highly active CO_2 electroreduction. *Nat. Commun.* **2025**, *16* (1), 1927.
(137) Wulan, B.; Cao, X.; Tan, D.; Ma, J.; Zhang, J. To Stabilize Oxygen on In/In2O3 Heterostructure via Joule Heating for Efficient Electrocatalytic CO_2 Reduction. *Adv. Funct. Mater.* **2023**, *33* (1), No. 2209114.
(138) Liu, K.; Shen, H.; Sun, Z.; Zhou, Q.; Liu, G.; Sun, Z.; Chen, W.; Gao, X.; Chen, P. Transient pulsed discharge preparation of graphene aerogel supports asymmetric Cu cluster catalysts promote CO_2 electroreduction. *Nat. Commun.* **2025**, *16* (1), 1203.
(139) Liu, K.; Sun, Z.; Chen, W.; Lang, X.; Gao, X.; Chen, P. Ultra-Fast Pulsed Discharge Preparation of Coordinatively Unsaturated Asymmetric Copper Single-Atom Catalysts for CO_2 Reduction. *Adv. Funct. Mater.* **2024**, *34* (16), No. 2312589.
(140) Shields, B. J.; Stevens, J.; Li, J.; Parasram, M.; Damani, F.; Alvarado, J. I. M.; Janey, J. M.; Adams, R. P.; Doyle, A. G. Bayesian reaction optimization as a tool for chemical synthesis. *Nature* **2021**, *590* (7844), 89−96.
(141) Yang, H.; Ren, G.; Li, Z.; Zhang, Z.; Meng, X. Fast Joule heating for transformation of Fe-MIL-125(Ti) to Fe/TiO_2 with enhanced photocatalytic activity in N2 fixation. *Applied Catalysis B: Environment and Energy* **2024**, *347*, No. 123795.
(142) Ren, G.; Zhao, Z.; Li, Z.; Zhang, Z.; Meng, X. Rapid Joule-Heating fabrication of oxygen vacancies and anchor of Ru clusters onto $BiVO_4$ for greatly enhanced photocatalytic N_2 fixation. *J. Catal.* **2023**, *428*, 115147.
(143) Fan, M.; Chang, X.; Meng, Q.; Wan, L. J.; Guo, Y. G. Progress in the sustainable recycling of spent lithium-ion batteries. *SusMat* **2021**, *1* (2), 241−254.
(144) Zhang, H.; Song, Y.; Zhao, J.; Cheng, Z.; Guo, J.; Cao, M.; Yu, H.; Wang, H.; Qie, L.; Yuan, L.; et al. Kinetics Dominated, Interface Targeted Rapid Heating for Battery Material Rejuvenation. *Adv. Energy Mater.* **2025**, *15* (13), No. 2404838.
(145) Tang, Y.; Xie, H.; Zhang, B.; Chen, X.; Zhao, Z.; Qu, J.; Xing, P.; Yin, H. Recovery and regeneration of $LiCoO_2$-based spent lithium-ion batteries by a carbothermic reduction vacuum pyrolysis approach: Controlling the recovery of CoO or Co. *Waste Manag* **2019**, *97*, 140−148.
(146) Hu, X.; Mousa, E.; Tian, Y.; Ye, G. Recovery of Co, Ni, Mn, and Li from Li-ion batteries by smelting reduction - Part I: A laboratory-scale study. *J. Power Sources* **2021**, *483*, No. 228936.
(147) Zhou, M.; Li, B.; Li, J.; Xu, Z. Pyrometallurgical Technology in the Recycling of a Spent Lithium Ion Battery: Evolution and the Challenge. *ACS ES&T Eng.* **2021**, *1* (10), 1369−1382.
(148) Shi, J.; Peng, C.; Chen, M.; Li, Y.; Eric, H.; Klemettinen, L.; Lundström, M.; Taskinen, P.; Jokilaakso, A. Sulfation Roasting Mechanism for Spent Lithium-Ion Battery Metal Oxides Under SO_2-O_2-Ar Atmosphere. *JOM* **2019**, *71* (12), 4473−4482.
(149) Li, L.; Fan, E.; Guan, Y.; Zhang, X.; Xue, Q.; Wei, L.; Wu, F.; Chen, R. Sustainable Recovery of Cathode Materials from Spent Lithium-Ion Batteries Using Lactic Acid Leaching System. *ACS Sustainable Chem. Eng.* **2017**, *5* (6), 5224−5233.
(150) Chagnes, A.; Pospiech, B. A brief review on hydrometallurgical technologies for recycling spent lithium-ion batteries. *J. Chem. Technol. Biotechnol.* **2013**, *88* (7), 1191−1199.
(151) Yu, H.; Huang, M.; Li, Y.; Chen, L.; Lv, H.; Yang, L.; Luo, X. Toward Joule heating recycling of spent lithium-ion batteries: A rising direct regeneration method. *J. Energy Chem.* **2025**, *105*, 501−513.
(152) Zhang, B.; Wang, L.; Song, D.; Wu, J.; Yu, J.; Li, J. Recycling of spent lithium-ion batteries via sulfidation shock. *Chem. Eng. J.* **2025**, *505*, No. 159206.
(153) Chen, W.; Salvatierra, R. V.; Li, J. T.; Kittrell, C.; Beckham, J. L.; Wyss, K. M.; La, N.; Savas, P. E.; Ge, C.; Advincula, P. A.; et al. Flash Recycling of Graphite Anodes. *Adv. Mater.* **2023**, *35* (8), No. e2207303.
(154) Chen, W.; Chen, J.; Bets, K. V.; Salvatierra, R. V.; Wyss, K. M.; Gao, G.; Choi, C. H.; Deng, B.; Wang, X.; Li, J. T.; et al. Battery metal recycling by flash Joule heating. *Sci. Adv.* **2023**, *9* (39), No. eadh5131.
(155) Zhu, X. H.; Li, Y. J.; Gong, M. Q.; Mo, R.; Luo, S. Y.; Yan, X.; Yang, S. Recycling Valuable Metals from Spent Lithium-Ion Batteries Using Carbothermal Shock Method. *Angew. Chem., Int. Ed. Engl.* **2023**, *62* (15), No. e202300074.
(156) Ma, J.; Wang, J.; Jia, K.; Liang, Z.; Ji, G.; Zhuang, Z.; Zhou, G.; Cheng, H. M. Adaptable Eutectic Salt for the Direct Recycling of Highly Degraded Layer Cathodes. *J. Am. Chem. Soc.* **2022**, *144* (44), 20306−20314.

https://doi.org/10.1021/acsnano.5c04768
ACS Nano XXXX, XXX, XXX−XXX

(157) Nie, H.; Xu, L.; Song, D.; Song, J.; Shi, X.; Wang, X.; Zhang, L.; Yuan, Z. $LiCoO_2$: recycling from spent batteries and regeneration with solid state synthesis. *Green Chem.* **2015**, *17* (2), 1276−1280.
(158) Xu, P.; Yang, Z.; Yu, X.; Holoubek, J.; Gao, H.; Li, M.; Cai, G.; Bloom, I.; Liu, H.; Chen, Y.; et al. Design and Optimization of the Direct Recycling of Spent Li-Ion Battery Cathode Materials. *ACS Sustainable Chem. Eng.* **2021**, *9* (12), 4543−4553.
(159) Yin, Y.-C.; Li, C.; Hu, X.; Zuo, D.; Yang, L.; Zhou, L.; Yang, J.; Wan, J. Rapid, Direct Regeneration of Spent $LiCoO_2$ Cathodes for Li-Ion Batteries. *ACS Energy Lett.* **2023**, *8* (7), 3005−3012.
(160) Guo, Y.; Yao, Y.; Guo, C.; Song, Y.; Huang, P.; Liao, X.; He, K.; Zhang, H.; Liu, H.; Hu, R.; et al. Atomistic Observation and Transient Reordering of Antisited Li/Fe Defects toward Sustainable $LiFePO_4$. *Energy Environ. Sci.* **2024**, *17*, 7749−7761.
(161) Du, K.; Ang, E. H.; Wu, X.; Liu, Y. Progresses in Sustainable Recycling Technology of Spent Lithium-Ion Batteries. *Energy Environ. Mater.* **2022**, *5* (4), 1012−1036.
(162) Natarajan, S.; Boricha, A. B.; Bajaj, H. C. Recovery of value-added products from cathode and anode material of spent lithium-ion batteries. *Waste Manag* **2018**, *77*, 455−465.
(163) Wang, H.; Huang, Y.; Huang, C.; Wang, X.; Wang, K.; Chen, H.; Liu, S.; Wu, Y.; Xu, K.; Li, W. Reclaiming graphite from spent lithium ion batteries ecologically and economically. *Electrochim. Acta* **2019**, *313*, 423−431.
(164) Chen, M.; Ma, X.; Chen, B.; Arsenault, R.; Karlson, P.; Simon, N.; Wang, Y. Recycling End-of-Life Electric Vehicle Lithium-Ion Batteries. *Joule* **2019**, *3* (11), 2622−2646.
(165) Liang, H.-J.; Hou, B.-H.; Li, W.-H.; Ning, Q.-L.; Yang, X.; Gu, Z.-Y.; Nie, X.-J.; Wang, G.; Wu, X.-L. Staging Na/K-ion de-/intercalation of graphite retrieved from spent Li-ion batteries: in operando X-ray diffraction studies and an advanced anode material for Na/K-ion batteries. *Energy Environ. Sci.* **2019**, *12* (12), 3575−3584.
(166) Da, H.; Gan, M.; Jiang, D.; Xing, C.; Zhang, Z.; Fei, L.; Cai, Y.; Zhang, H.; Zhang, S. Epitaxial Regeneration of Spent Graphite Anode Material by an Eco-friendly In-Depth Purification Route. *ACS Sustainable Chem. Eng.* **2021**, *9* (48), 16192−16202.
(167) Dong, S.; Song, Y.; Ye, K.; Yan, J.; Wang, G.; Zhu, K.; Cao, D. Ultra-fast, low-cost, and green regeneration of graphite anode using flash joule heating method. *EcoMat* **2022**, *4* (5), No. e12212.
(168) Yi, C.; Ge, P.; Wu, X.; Sun, W.; Yang, Y. Tailoring carbon chains for repairing graphite from spent lithium-ion battery toward closed-circuit recycling. *J. Energy Chem.* **2022**, *72*, 97−107.
(169) Saadi, M. A. S. R.; Advincula, P. A.; Thakur, M. S. H.; Khater, A. Z.; Saad, S.; Shayesteh Zeraati, A.; Nabil, S. K.; Zinke, A.; Roy, S.; Lou, M.; et al. Sustainable valorization of asphaltenes via flash joule heating. *Sci. Adv.* **2022**, *8* (46), No. eadd3555.
(170) Andersen, H. L.; Djuandhi, L.; Mittal, U.; Sharma, N. Strategies for the Analysis of Graphite Electrode Function. *Adv. Energy Mater.* **2021**, *11* (48), No. 2102693.
(171) Wang, M.; Wang, J.; Xiao, J.; Ren, N.; Pan, B.; Chen, C. S.; Chen, C. H. Introducing a Pseudocapacitive Lithium Storage Mechanism into Graphite by Defect Engineering for Fast-Charging Lithium-Ion Batteries. *ACS Appl. Mater. Interfaces* **2022**, *14* (14), 16279−16288.
(172) LeGe, N.; He, X.-X.; Wang, Y.-X.; Lei, Y.; Yang, Y.-X.; Xu, J.-T.; Liu, M.; Wu, X.; Lai, W.-H.; Chou, S.-L. Reappraisal of hard carbon anodes for practical lithium/sodium-ion batteries from the perspective of full-cell matters. *Energy Environ. Sci.* **2023**, *16* (12), 5688−5720.
(173) Luo, J.; Zhang, J.; Guo, Z.; Liu, Z.; Dou, S.; Liu, W.-D.; Chen, Y.; Hu, W. Recycle spent graphite to defect-engineered, high-power graphite anode. *Nano Res.* **2023**, *16* (4), 4240−4245.
(174) Weng, S.; Wu, S.; Liu, Z.; Yang, G.; Liu, X.; Zhang, X.; Zhang, C.; Liu, Q.; Huang, Y.; Li, Y.; et al. Localized-domains staging structure and evolution in lithiated graphite. *Carbon Energy* **2023**, *5* (1), No. e224.
(175) He, Y.; Liu, Z.; Zhou, G.; Wang, H.; Bai, C.; Rodney, D.; Appel, F.; Xu, D.; Yang, R. Dislocation dipole-induced strengthening in intermetallic TiAl. *Scr. Mater.* **2018**, *143*, 98−102.
(176) Cheng, Z.; Luo, Z.; Zhang, H.; Zhang, W.; Gao, W.; Zhang, Y.; Qie, L.; Yao, Y.; Huang, Y.; Fu, K. K. Targeted regeneration and upcycling of spent graphite by defect-driven tin nucleation. *Carbon Energy* **2024**, *6* (4), e395.
(177) Liu, K.; Yang, S.; Luo, L.; Pan, Q.; Zhang, P.; Huang, Y.; Zheng, F.; Wang, H.; Li, Q. From spent graphite to recycle graphite anode for high-performance lithium ion batteries and sodium ion batteries. *Electrochim. Acta* **2020**, *356*, No. 136856.
(178) Yang, Y.; Song, S.; Lei, S.; Sun, W.; Hou, H.; Jiang, F.; Ji, X.; Zhao, W.; Hu, Y. A process for combination of recycling lithium and regenerating graphite from spent lithium-ion battery. *Waste Manag* **2019**, *85*, 529−537.
(179) Lv, W.; Wang, Z.; Cao, H.; Sun, Y.; Zhang, Y.; Sun, Z. A Critical Review and Analysis on the Recycling of Spent Lithium-Ion Batteries. *ACS Sustainable Chem. Eng.* **2018**, *6* (2), 1504−1521.
(180) Ma, X.; Chen, M.; Chen, B.; Meng, Z.; Wang, Y. High-Performance Graphite Recovered from Spent Lithium-Ion Batteries. *ACS Sustainable Chem. Eng.* **2019**, *7* (24), 19732−19738.
(181) Yang, J.; Fan, E.; Lin, J.; Arshad, F.; Zhang, X.; Wang, H.; Wu, F.; Chen, R.; Li, L. Recovery and Reuse of Anode Graphite from Spent Lithium-Ion Batteries via Citric Acid Leaching. *ACS Appl. Energy Mater.* **2021**, *4* (6), 6261−6268.
(182) Lee, J.; Jin, D.; Kim, J. Y.; Roh, Y.; Lee, H.; Kang, S. H.; Choi, J.; Jo, T.; Lee, Y. G.; Lee, Y. M. Dry Pre-Lithiation for Graphite-Silicon Diffusion-Dependent Electrode for All-Solid-State Battery. *Adv. Energy Mater.* **2023**, *13* (25), No. 2300172.
(183) Jin, L.; Shen, C.; Wu, Q.; Shellikeri, A.; Zheng, J.; Zhang, C.; Zheng, J. P. Pre-Lithiation Strategies for Next-Generation Practical Lithium-Ion Batteries. *Adv. Sci. (Weinh)* **2021**, *8* (12), No. e2005031.
(184) Yang, C.; Ma, H.; Yuan, R.; Wang, K.; Liu, K.; Long, Y.; Xu, F.; Li, L.; Zhang, H.; Zhang, Y.; et al. Roll-to-roll prelithiation of lithium-ion battery anodes by transfer printing. *Nat. Energy* **2023**, *8* (7), 703−713.
(185) Fan, X.; Chen, L.; Borodin, O.; Ji, X.; Chen, J.; Hou, S.; Deng, T.; Zheng, J.; Yang, C.; Liou, S. C.; et al. Non-flammable electrolyte enables Li-metal batteries with aggressive cathode chemistries. *Nat. Nanotechnol.* **2018**, *13* (8), 715−722.
(186) Gao, Y.; Yan, Z.; Gray, J. L.; He, X.; Wang, D.; Chen, T.; Huang, Q.; Li, Y. C.; Wang, H.; Kim, S. H.; et al. Polymer-inorganic solid-electrolyte interphase for stable lithium metal batteries under lean electrolyte conditions. *Nat. Mater.* **2019**, *18* (4), 384−389.
(187) Sun, J.; Zhang, S.; Li, J.; Xie, B.; Ma, J.; Dong, S.; Cui, G. Robust Transport: An Artificial Solid Electrolyte Interphase Design for Anode-Free Lithium-Metal Batteries. *Adv. Mater.* **2023**, *35* (20), No. e2209404.
(188) Zou, F.; Nallan, H. C.; Dolocan, A.; Xie, Q.; Li, J.; Coffey, B. M.; Ekerdt, J. G.; Manthiram, A. Long-life $LiNi_{0.5}Mn_{1.5}O_4$/graphite lithium-ion cells with an artificial graphite-electrolyte interface. *Energy Storage Mater.* **2021**, *43*, 499−508.
(189) Ji, Y.; Zhang, H.; Yang, D.; Pan, Y.; Zhu, Z.; Qi, X.; Pi, X.; Du, W.; Cheng, Z.; Yao, Y.; et al. Regenerated Graphite Electrodes with Reconstructed Solid Electrolyte Interface and Enclosed Active Lithium Toward > 100% Initial Coulombic Efficiency. *Adv. Mater.* **2024**, *36*, No. e2312548.
(190) Zhang, H.; Ji, Y.; Yao, Y.; Qie, L.; Cheng, Z.; Ma, Z.; Qian, X.; Yang, R.; Li, C.; Guo, Y.; et al. Transient and dry recycling of battery materials with negligible carbon footprint and roll-to-roll scalability. *Energy Environ. Sci.* **2023**, *16* (6), 2561−2571.
(191) Yang, Y.; Huang, G.; Xu, S.; He, Y.; Liu, X. Thermal treatment process for the recovery of valuable metals from spent lithium-ion batteries. *Hydrometallurgy* **2016**, *165*, 390−396.
(192) Liu, K.; Yang, S.; Lai, F.; Wang, H.; Huang, Y.; Zheng, F.; Wang, S.; Zhang, X.; Li, Q. Innovative Electrochemical Strategy to Recovery of Cathode and Efficient Lithium Leaching from Spent Lithium-Ion Batteries. *ACS Appl. Energy Mater.* **2020**, *3* (5), 4767−4776.
(193) Chen, X.; Li, S.; Wu, X.; Zhou, T.; Ma, H. In-situ recycling of coating materials and Al foils from spent lithium ion batteries by

https://doi.org/10.1021/acsnano.5c04768
ACS Nano XXXX, XXX, XXX−XXX

ultrasonic-assisted acid scrubbing. *J. Cleaner Prod.* **2020**, *258*, No. 120943.
(194) Yang, C.; Yao, Y.; He, S.; Xie, H.; Hitz, E.; Hu, L. Ultrafine Silver Nanoparticles for Seeded Lithium Deposition toward Stable Lithium Metal Anode. *Adv. Mater.* **2017**, *29* (38), No. 1702714.
(195) Zhu, X.; Lin, L.; Pang, M.; Jia, C.; Xia, L.; Shi, G.; Zhang, S.; Lu, Y.; Sun, L.; Yu, F.; et al. Continuous and low-carbon production of biomass flash graphene. *Nat. Commun.* **2024**, *15* (1), 3218.
(196) Cheng, Z.; Zhang, H.; Cui, J.; Zhao, J.; Dai, S.; Zhang, Z.; Song, K.; Wang, S.; Yuan, Y.; Chen, Q.; et al. Interlayer-expanded carbon anodes with exceptional rates and long-term cycling via kinetically decoupled carbonization. *Joule* **2025**, *9* (3), No. 101812.
(197) Dong, Q.; Hu, S.; Hu, L. Electrothermal synthesis of commodity chemicals. *Nature Chemical Engineering* **2024**, *1*, 680.
(198) Wyss, K. M.; De Kleine, R. D.; Couvreur, R. L.; Kiziltas, A.; Mielewski, D. F.; Tour, J. M. Upcycling end-of-life vehicle waste plastic into flash graphene. *Commun. Eng.* **2022**, *1* (1), 3.
(199) Wang, A. E. M.; Lee, U.; Bafana, A.; Benavides, P. T.; Burnham, A.; C, H.; Dai, Q.; Ulises, R.; Gracida-Alvarez, T.; Hawkins, R.; Paola Vega Jaquez, J. C. K.; Kwon, H.; Lu, Z.; Liu, X.; Ou, L.; Pingping Sun, O. W.; Xu, H.; Yoo, E.; George, G.; Guiyan Zang, Z. *Summary of Expansions and Updates in GREET 2020*; Argonne National Lab. (ANL): 2020.
(200) Qiang Dai, J. S.; Ahmed, S.; Gaines, L.; Jarod, C. K.; Wang, M. *Everbatt: A Closed-Loop Battery Recycling Costa and Environmental Impacts Model*; Argonne National Lab. (ANL): 2019.

https://doi.org/10.1021/acsnano.5c04768
ACS Nano XXXX, XXX, XXX−XXX